Fusion of ^{16}O + ^{40}Ca at $E_{\text{lab}}(^{16}\text{O}) = 13.4$ MeV/nucleon

C. Beck,* D. G. Kovar, S. J. Sanders, B. D. Wilkins, D. J. Henderson, R. V. F. Janssens,
W. C. Ma, M. F. Vineyard,† and T. F. Wang
Physics Division, Argonne National Laboratory, Argonne, Illinois 60439

C. F. Maguire
Vanderbilt University, Nashville, Tennessee 37235

F. W. Prosser
University of Kansas, Lawrence, Kansas 66045

G. Rosner‡
Technische Universität München, Garching, Federal Republic of Germany
(Received 23 May 1988; revised manuscript received 25 November 1988)

Mass and velocity distributions have been measured for the evaporation residue and fusion-fission products from the ^{16}O + ^{40}Ca reaction at 214 MeV. Comparisons of Monte Carlo statistical evaporation simulations to the observed angle and mass dependences of the evaporation-residue velocity distributions were used to set limits on the maximum complete-fusion cross section and to extract information about the magnitude and character of incomplete-fusion processes. The extracted value of the complete fusion evaporation-residue cross section is discussed in the framework of previous results and existing models.

I. INTRODUCTION

For heavy-ion induced reactions at bombarding energies $E_{\text{lab}} > 10$ MeV/nucleon there is experimental evidence that incomplete-fusion reactions occur.[1-5] These processes are understood to take place when a nucleon (or nucleons) is (are) emitted from the projectile or target prior to the fusing of the remaining nucleons. Whether these reactions are governed by the entrance-channel dynamics, by the competition with preequilibrium processes, or by the properties of the composite system is not clearly established. The resulting "compound nucleus" is lighter than the projectile plus target composite system and moves with a different velocity because of the linear momentum removed by the emitted nucleon(s). The clearest evidence for such processes comes from (i) measurements of the velocity distributions of evaporation residues[1,3] and (ii) from folding angle measurements of fission fragments.[2,3] These data show that with increasing bombarding energies there is a decreasing probability that the fusion products originate from a composite system which has received the full linear momentum of the projectile. In fact, at $E_{\text{lab}} > 35$ MeV/nucleon there is essentially no cross section consistent with complete fusion.[1-5] Between 10 and 35 MeV/nucleon only limits of the maximum cross section consistent with complete fusion have been extracted.

Unfortunately, the mass and velocity (or folding angle) distributions for evaporation residues (or fission fragments) arising from complete fusion and from incomplete-fusion overlap in mass and velocity (or folding angle) and one is forced to use decomposition procedures to extract cross sections. Although exclusive

measurements will be necessary to provide the constraints to identify the reaction processes, at present there is a need for guidance as to what features in the data should be focussed upon.

In the present study of the ^{16}O + ^{40}Ca reaction at $E_{\text{lab}} = 214$ MeV inclusive measurements of the velocity distributions of the mass-resolved reaction products were performed. The yields associated with evaporation residues and binary processes were identified. The measurements provided information on the angle and mass dependence of the evaporation-residue velocity spectra. The analysis focuses on a detailed comparison between observed behaviors and those predicted by Monte Carlo simulations of complete fusion. It identifies where discrepancies occur and, within this framework, establishes cross section limits.

The results of this analysis indicate that the evaporation-residue velocity spectra as a function of angle and mass contain information about the relative contributions of single-nucleon, two-nucleon, and multinucleon preequilibrium processes. Furthermore, it was found that some aspects of the evaporation-residue data which deviate from the simulations may result from heavy-particle evaporation rather than from incomplete fusion processes. Our decomposition of the velocity spectra and extraction of an upper limit for the complete-fusion cross section resolves some of the discrepancies reported in the literature[6] between the evaporation-residue cross sections for the mass-asymmetric entrance-channel reaction ^{16}O + ^{40}Ca (Ref. 7) and the more symmetric entrance-channel reactions ^{28}Si + ^{28}Si,[8] and ^{32}S + ^{24}Mg (Ref. 9) which form the same compound nucleus ^{56}Ni. It leaves unresolved questions regarding the existence of an

entrance channel mass-asymmetry dependence of incomplete-fusion processes which has been suggested from systematics.

The details of the experimental method are presented in Sec. II. In Sec. III, the experimental results for the elastic scattering, the evaporation residues, and the fission-like fragments are presented. The analysis of the evaporation-residue yields and the separation of these into complete- and incomplete-fusion components are presented in Sec. IV. The main features of the incomplete- and complete-fusion yields are discussed in the context of previously reported results and recent fusion models in Sec. V. The summary and conclusion of this study are presented in Sec. VI.

II. EXPERIMENTAL PROCEDURE

The measurements were performed using a 214-MeV ^{16}O beam from the Argonne National Laboratory AT-LAS facility. The target was a self-supporting (685 μg/cm^2), isotopically enriched (99.9%), ^{40}Ca foil mount-

ed in the ATLAS 36-inch scattering chamber. The reaction products were detected in an array of four ΔE-E Si telescopes and one E Si detector mounted in the angular range 2°–52°. The most forward two detectors were mounted at 87 and 73 cm, respectively, from the target. The three larger angle detectors were positioned at distances ranging from 35 to 40 cm. Mass identification was obtained by the time-of-flight technique using the RF beam timing of ATLAS. Examples of the mass identifications achieved are shown in Figs. 1 and 2. The time resolution of the ^{16}O beam pulses was better than 150 ps (FWHM) with a period of 247.4 ns between pulses.

A monitor detector located out of plane ($\theta=4.5°$, $\phi=4.4°$) was used to establish the relative normalization. This normalization was found to be in excellent agreement with that obtained using a Faraday cup beam integrator. The absolute normalization of the differential cross sections was determined using an optical-model fit to the measured ^{16}O+^{40}Ca elastic scattering distribution at $E_{\text{lab}}=214$ MeV (to be discussed in Sec. III A).

The detector angles and solid angles, established from

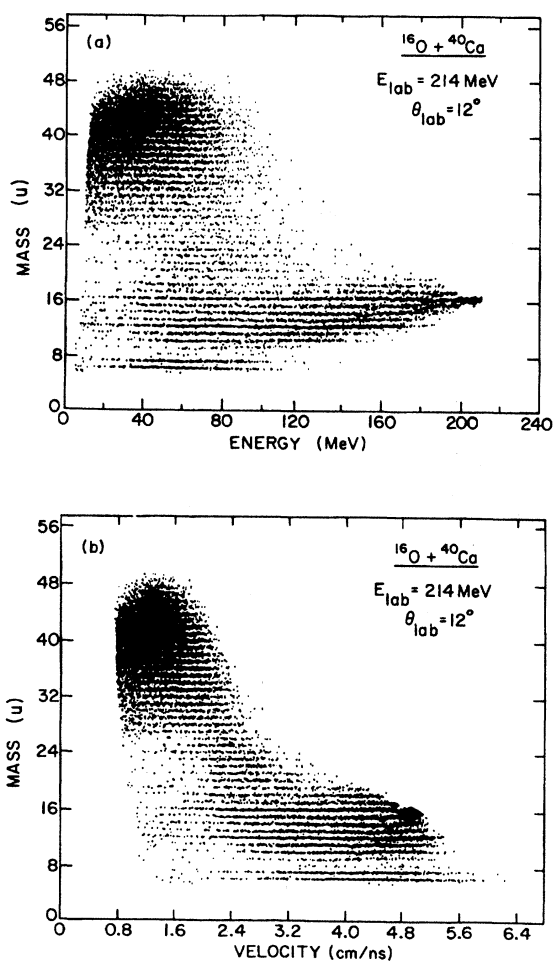FIG. 1. (a) Two dimensional mass versus total-energy spectrum for ^{16}O+^{40}Ca at $E_{\text{lab}}=214$ MeV and $\theta_{\text{lab}}=12°$. (b) Two-dimensional mass versus velocity spectrum for ^{16}O+^{40}Ca at $E_{\text{lab}}=214$ MeV and $\theta_{\text{lab}}=12°$.
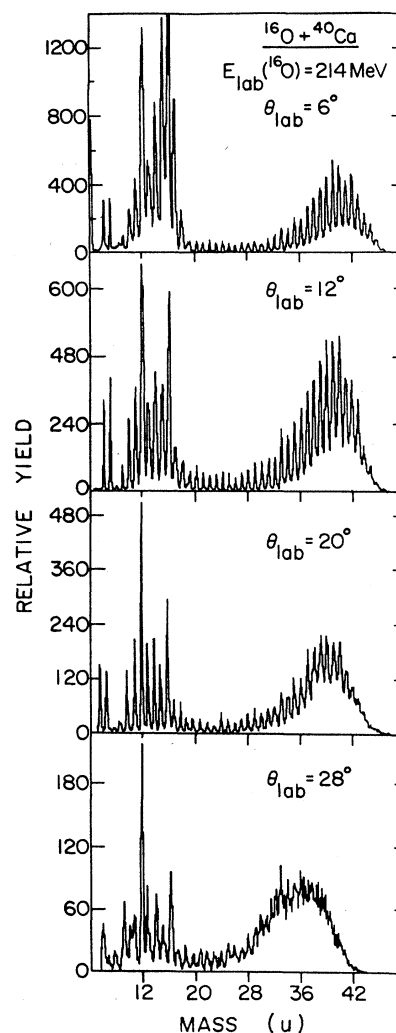

FIG. 2. Mass spectra observed at laboratory angles of 6° and 12° (TOF 1), 20° (TOF 2), and 28° (TOF 3).

C. BECK *et al.*

the geometry, were checked using the elastic scattering of ^{16}O and ^{32}S from a ^{197}Au target. At $E_{\mathrm{lab}}=214$ MeV, small angle $(2°-5°)$ ^{16}O elastic scattering measurements on either side of the beam axis established an angular shift from the optical alignment geometry of $0.10°\pm0.02°$. At lower bombarding energies, using ^{16}O (59.5 MeV) and ^{32}S (121 MeV) beams, the relative angles between the detectors and the relative solid angles were checked by measuring elastic scattering yields of known cross sections.

The energy and time calibrations of the detectors were determined using the elastic scattering of ^{16}O (59.5 and 214 MeV) and ^{32}S (121 and 142 MeV) ions from an ^{197}Au target, and using the 5.486 MeV alpha group from an ^{241}Am source. Each measured fragment energy was corrected event by event for energy losses in the target and the gold dead-layer of the Si detector, and for the pulse-height defect[10−12] in the silicon detectors. The pulse-height correction of Kaufman, *et al.*,[10] was used, where the scaling factor was established for each Si detector using the pulse heights induced by the fission fragments of ^{252}Cf. The prescription of Ogihara, *et al.*[11] was found to give similar corrections to the experimental data; on the other hand, the parametrization of Moulton *et al.*[12] seems to be inappropriate for the evaporation-residue fragments produced in the present reaction. Plasma-delay corrections[13,14] were applied to the timing measurement of each detector following the set of empirical formulae established by Bohne, *et al.*[13]

The velocities of the reaction products were extracted event by event using two complementary methods: (1) by direct time-of-flight measurement corrected for plasma delay, and (2) using the measured energies corrected for pulse-height defect together with the mass identification. These methods gave equivalent results to within 0.5%. The velocity spectra presented in this paper have been obtained from the energy measurements. Based on the uncertainties associated with the energy corrections and of the energy calibration of the low-energy beams (known to an accuracy of about 0.3%), the evaporation-residue velocities are believed to be determined to ±0.015 cm/ns.

III. EXPERIMENTAL RESULTS

A. Elastic scattering

The elastic scattering of ^{16}O + ^{40}Ca at $E_{\mathrm{lab}}=214$ MeV was measured using the three most forward angle time-of-flight detectors. The extracted angular distribution shown in Fig. 3 is in excellent agreement with that reported by Vigdor, *et al.*[7] The solid line represents the results of an optical-model calculation performed with the code PTOLEMY[15] using parameter set 2a of Vigdor, *et al.* Based on the optical-model analysis of the elastic-scattering angular distribution, the total reaction cross section for ^{16}O + ^{40}Ca scattering is 2110 ± 100 mb.

B. Evaporation residues

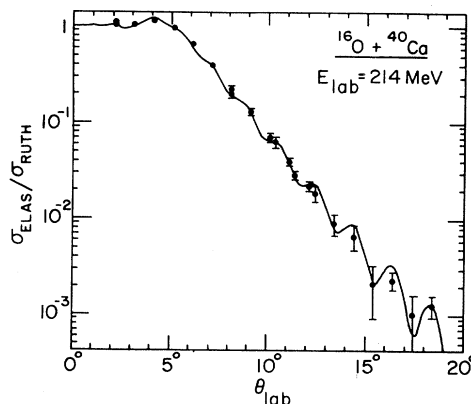The detected evaporation-residue fragments extend over large mass $(32 < A < 52)$ and energy $(10$

FIG. 3. Elastic scattering angular distribution measured for ^{16}O + ^{40}Ca at $E_{\mathrm{lab}}=214$ MeV. The solid curve is a PTOLEMY optical-model calculation obtained using potential 2a of Ref. 7.

$< E_{\mathrm{residue}} < 90$ MeV) ranges. (See Fig. 1.) For the lower evaporation-residue masses there is clear evidence of a reaction component which does not follow the average velocity of the center of mass. For even smaller masses $(A < 32)$, this second component dominates the spectrum and, as will be shown, is characteristic of a fully energy-damped, binary-reaction process. In Fig. 4 the velocity
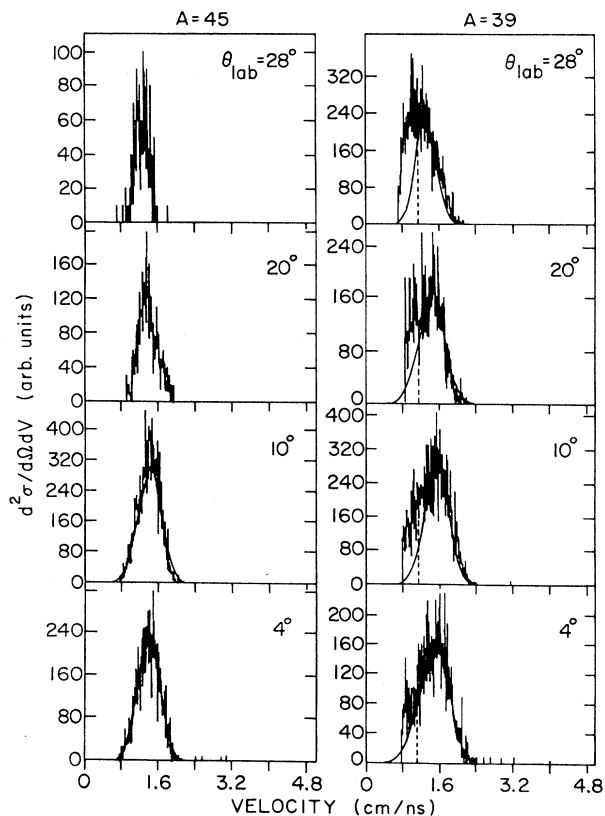

FIG. 4. Inclusive velocity spectra for $A = 39$ and 45. The solid curves and dashed lines are, respectively, the Gaussian fits using the high-velocity shoulder and the velocity cuts used to obtain angular distributions for the evaporation-residue yields.

spectra observed for $A = 45$ can be seen to remain Gaussian as a function of angle, typical of what is observed for the heavier evaporation-residue masses, while the velocity spectra for $A = 39$ show evidence of an additional lower velocity component which becomes more pronounced at larger angles.

To extract cross sections, the Galilean-invariant cross sections [$(1/v^2)d^2\sigma/d\Omega dv$] for the evaporation residues were assumed to have a Gaussian shaped distribution, with a possible shift of the centroid with respect to that expected for complete fusion. For masses $A > 39$ this procedure clearly identifies the evaporation-residue component. For lighter masses ($A < 39$) at larger angles uncertainties are associated with this procedure. For $\theta_{lab} > 28°$, because of the statistics and the additional reaction components, it becomes increasingly difficult to identify a Gaussian component in the spectra and, even when a Gaussian component is apparent, it is difficult to estimate the "background" contributions. In these cases, the extracted yields are upper limits on the evaporation-residue yields. Because of the relatively small contributions to the total cross section, the uncertainties in these channels do not significantly influence the summed evaporation-residue angular distributions and extracted cross sections.

The angle dependence of the extracted evaporation-residue velocity centroids, expressed in terms of $R_v = v_{centroid}/(v_{c.m.} \cos\theta_{lab})$ (where $v_{c.m.}$ is the center-of-mass velocity for the system and θ_{lab} is the laboratory angle at which the centroid is observed), is shown in Fig. 5 for representative masses. The velocity $v_{c.m.} \cos\theta_{lab}$ is the average velocity expected for evaporation residues produced in a complete-fusion reaction, where the evaporated light particles are emitted isotropically in the frame of the compound nucleus with Maxwellian velocity distributions.[16] The shift in the evaporation-residue centroids from that expected for complete fusion ($R_v = 1$) is greatest for the lower masses: an average shift of 16% is observed for $A = 39$ as compared 9% for $A = 48$. In Fig. 6 the centroid behavior is plotted as a function of mass for various representative angles. Although the average centroids (indicated by the dashed lines) fall generally within the uncertainties associated with the individual centroids extracted, a shift to lower velocities with decreasing evaporation-residue mass is apparent, starting in the mass region $40 < A < 45$. The average centroid, obtained by averaging over $40 < A < 50$ and $2° < \theta_{lab} < 28°$, gives a value $\langle R_v \rangle = 0.885 \pm 0.020$, in agreement with the measurement of Chan et al.[1,17] for ^{16}O$+^{40}$Ca at 13.6 MeV ($\langle R_v \rangle = 0.89 \pm 0.06$) and consistent with the Viola systematics[2,18] derived from fission studies of heavier systems. The behavior as a function of angle is similar to that reported for the ^{16}O$+^{27}$Al reaction at 150 MeV.[19]

From the widths of the evaporation-residue invariant cross section velocity distributions the experimental standard deviations s_{ER} were extracted. In Fig. 7 the extracted s_{ER} at 6° and 11° are shown plotted as a function of the number of evaporated nucleons. The observed increment in s_{ER} of about 0.016 cm/ns/A is in agreement with that reported by Chan et al.[1] for systems of similar mass studied with ^{14}N, ^{19}F, and ^{20}Ne projectiles at bombarding

energies lower than 15 MeV/nucleon. The solid line is the result of LILITA[20] calculations which will be discussed in more detail in Sec. IV. The widths predicted by LILITA are significantly smaller than those observed for the lighter evaporation-residue masses.

The extracted evaporation-residue angular distributions for the individual mass groups, $32 \leq A \leq 49$, are shown in Fig. 8. The solid lines indicate the predicted shapes of the angular distributions from LILITA simulations and the dashed lines the fits to the experimental distributions used for integration of the cross sections. The mass-summed angular distribution ($32 \leq A \leq 49$) compared with the LILITA prediction is shown in Fig. 9. Also shown in the figure is the angular distribution extracted in this study for the total yield (also $32 \leq A \leq 52$), and the total evaporation-residue angular distribution reported by Vigdor et al.[7] [which agrees well with the shape of our total yields at smaller angles ($< 35°$)]. The predicted angular distributions shown in Figs. 8 and 9 are significantly narrower than those observed. The angle integrated mass distribution for the evaporation residues, $\sigma_{ER}(A)$, (Table I) is compared in Fig. 10 with that measured for the total yields ($A > 6$; excluding the elastic scattering yield), $\sigma_{TOT}(A)$. The extracted total yield
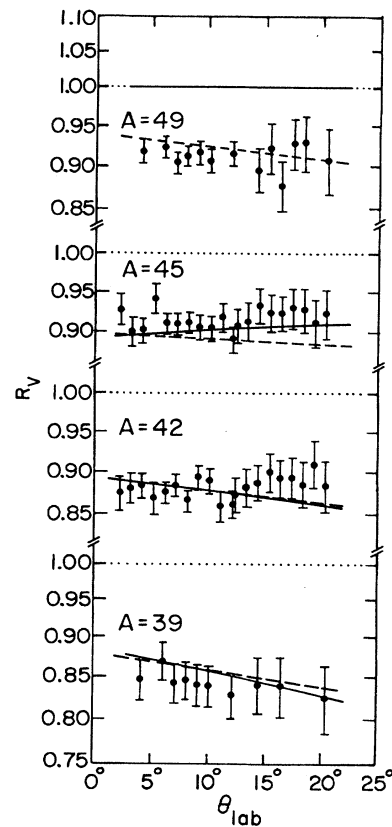

FIG. 5. Observed velocity-deficit fraction R_v plotted against laboratory angle for representative evaporation-residue masses. The solid curve is the velocity-deficit behavior predicted by the two-source simulation (^{16}O$+^{40}$Ca and ^{12}C $+^{40}$Ca), and the dashed line for the three-source simulations (^{16}O$+^{40}$Ca, ^{12}C $+^{40}$Ca, and ^{15}N$+^{40}$Ca) discussed in the text.
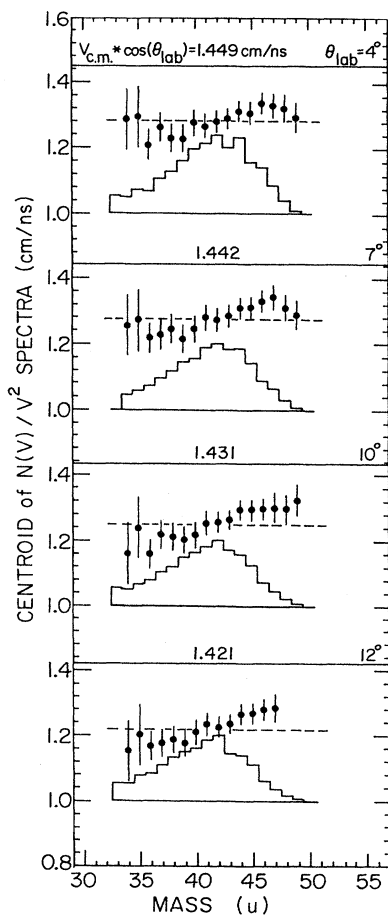
FIG. 6. Mass dependence of the velocity centroids measured at the indicated laboratory angles. The horizontal lines represent the compound-nucleus velocities for full linear-momentum transfer. The mass distributions observed are indicated by the histograms.
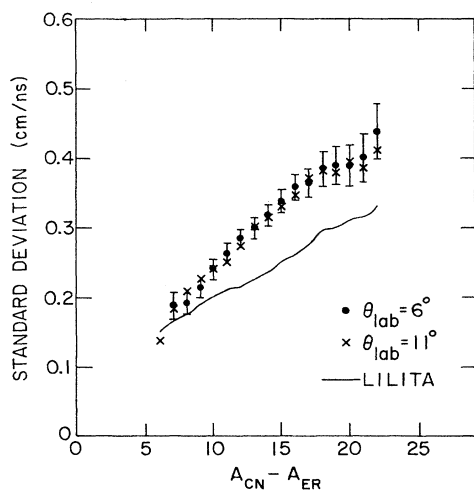
FIG. 7. Extracted standard deviation parameter s_{ER} at $6°$ (solid points) and $11°$ (crosses) as a function of the number of evaporated nucleons $A_{CN} - A_{ER}$. The solid line represents the predictions of the code LILITA at $10°$.
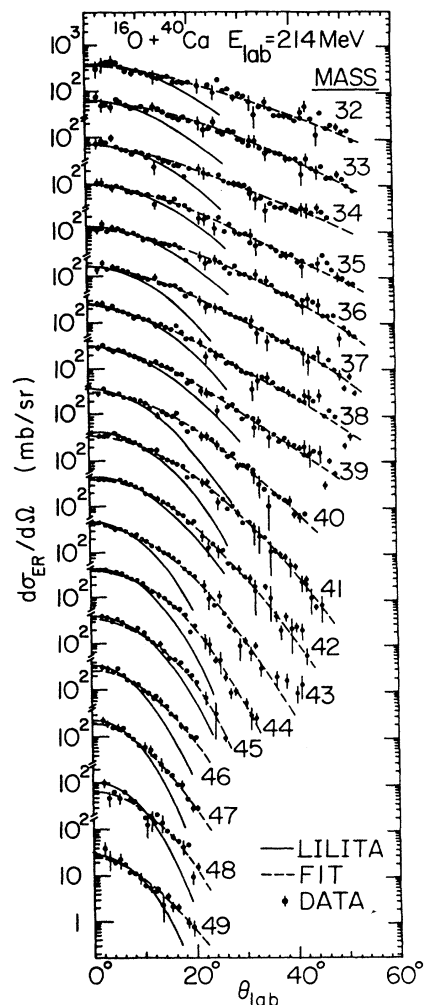
FIG. 8. Angular distributions extracted for the evaporation residues ($32 \leq A \leq 49$). The dashed lines are the fits to the data used to obtain the integrated cross sections. The solid lines are the angular distributions predicted by LILITA. (See text.)
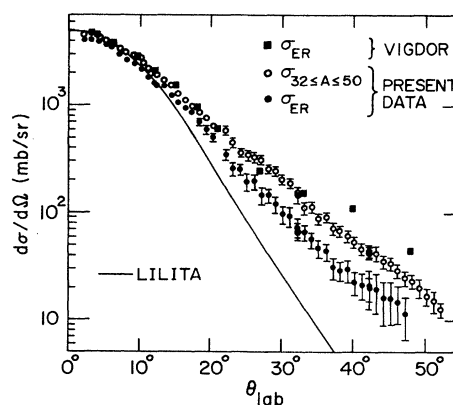
FIG. 9. Angular distributions of the total yields observed for $32 \leq A \leq 50$ (open circles) and of the yields identified as consistent with evaporation residues (solid circles) in the present measurement. The solid rectangles represent the data of Vigdor *et al.* (Ref. 7). The solid line represents the prediction of the code LILITA.
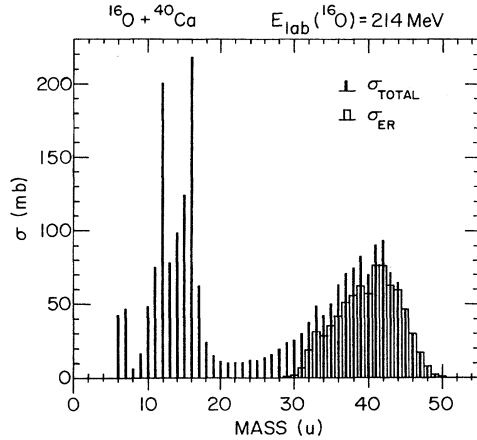
FIG. 10. Angle-integrated mass distribution of all fragments. The narrow, solid histograms represent the total yield cross sections; the open histograms are the evaporation-residue identified cross sections.

cross section of 2268±200 mb is similar in magnitude to the total reaction cross section deduced from the optical-model analysis of the elastic scattering data.

The total evaporation-residue cross section extracted from integration of the angular distributions is 762±100 mb. The uncertainty in the absolute cross section ($\sim 15\%$) arises from counting statistics, overall normalization uncertainties ($\pm 4\%$), extrapolations out of the measured angular range ($\pm 2\%$), and uncertainties in the decomposition procedure used to extract the yields. The evaporation-residue cross section can be compared to the total yield cross section of 965±100 mb observed in the same mass range (i.e., $32 \leq A \leq 52$). Our total yield cross section, although consistent with the value found by Vigdor et al.[7] (1127±100 mb), is approximately 150 mb smaller. The discrepancy results in part from a 5% difference in our absolute normalization and in part from the larger back-angle yields reported by Vigdor. The identification in the present analysis of 20% of the cross section with nonevaporation processes is similar to what was found by Rosner et al.[21] in an analysis of 216-MeV ^{19}F+^{40}Ca reaction data, where velocity spectra and heavy-ion heavy-ion coincidence data were used to show that 16% of the yield had a nonevaporation origin.

C. Fusion-fission yields

For lighter masses ($A < 32$) the average velocities are observed to be substantially greater than that of the compound nucleus, suggesting more binary reaction processes. The Q-value spectra display a bell-shaped structure characteristic of a fully damped process. Representative spectra observed at $\theta_{lab} = 18°$ are shown in Fig. 11. For $A = 20$ another component is seen at more positive Q values which probably arises from a combination of quasielastic and deep-inelastic processes. The broadened structure of the $A = 28$ energy spectrum can be explained by the two allowed kinematical solutions while the rapid falloff of the yields near $Q = -160$ MeV results from the experimental low-energy threshold. The most probable Q values range from $Q = -123.5$ MeV for $A = 28$, to

$Q = -115.0$ MeV for $A = 20$. These values are consistent with a fusion-fission mechanism ($-116 < Q < -110$ MeV) where the total fragment kinetic energy is taken as the sum of the Coulomb and rotation energy of the two fragments at the scission point. The observed $A = 28$ Q value corresponds to an average total kinetic energy (TKE) for symmetric mass splitting of $\langle$TKE$\rangle = 29.4 \pm 3.0$ MeV. Since no attempt was made to correct the experimental data for secondary light-particle emission from the primary fragments, it is not surprising that this $\langle$TKE$\rangle$ value is smaller than that observed at lower incident beam energies ($\langle$TKE$\rangle = 36$ MeV with $E_{c.m.} \simeq 60$ MeV) by Sanders et al.[22,23] The empirical ex-
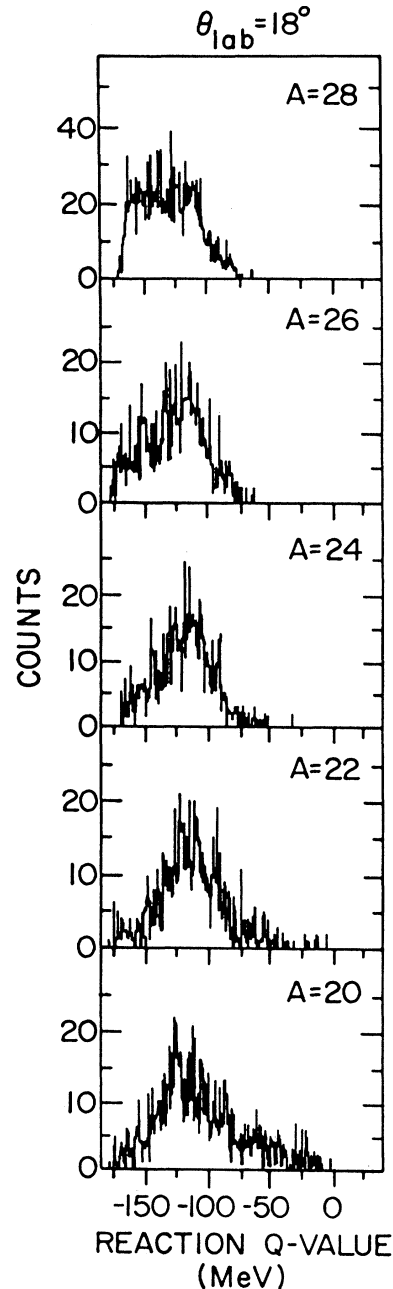

FIG. 11. Q-value spectra of the binary fragments observed at $\theta_{lab} = 18°$ for the indicated masses.

pressions of Viola *et al.*[24] ($\langle$TKE$\rangle=0.1189Z^2/A^{1/3}$ $+7.3$ MeV), and Töke *et al.*[25] ($\langle$TKE$\rangle=0.124Z^2/A^{1/3}$), based primarily on fission data from much heavier systems, predict $\langle$TKE$\rangle$ of 31.7 MeV and 25.4 MeV, respectively.

The center-of-mass angular distributions of the binary fragments are shown in Fig. 12. For $A>23$, constant cross sections of $d\sigma/d\theta$ can be observed, corresponding to $d\sigma/d\Omega\propto1/\sin\theta$. This is consistent with the behavior expected for the decay of a long-lived, composite, dinuclear system (or compound nucleus) with a lifetime comparable to or longer than the rotation period. For $20\le A\le23$ the $1/\sin\theta$ behavior ($d\sigma/d\theta=$constant) is still observed at larger angles, but at smaller angles more peripheral collisions with more positive Q values lead to faster rising angular distributions.

These observations are consistent with the presence of a fission component as has been previously reported in similar mass reactions.[22,26-30] The total fission-like integrated cross sections for resolved mass $20<A<28$ are shown in the insert of Fig. 13 compared to the results of Ref. 22 at $E_{lab}=76.9$ MeV ($E_{c.m.}=54.9$ MeV). To obtain the total cross sections, a $1/\sin\theta$ behavior with magnitude fixed by the larger angle data (see Fig. 12) was assumed. The summed ($20<A<28$) cross section

FIG. 13. Excitation function of the fission-like cross sections for masses $20\le A\le28$ observed in the $^{16}O+^{40}Ca$ reaction. The low-energy points are taken from Refs. 22 and 31. The solid curve is a guide to the eye. The fission-like mass distributions are shown in the inset for $E_{c.m.}=54$ MeV (Ref. 22) and 153 MeV (present work).

($\sigma_{fission}=98\pm10$ mb) obtained in our measurement at 214 MeV ($E_{c.m.}=152.9$ MeV) is shown in Fig. 13 with the data of Sanders *et al.*[22] and results[31] obtained at 148.6 MeV ($E_{c.m.}=106.1$ MeV). A rapid increase of the cross section above the s-wave fission barrier (at $E_{c.m.}=45.9$ MeV) is observed, followed by a plateau as expected for a compound-nucleus decay process. A similar overall energy dependence has been reported recently for the $^{12}C+^{40}Ca$ reaction[29] with, however, substantially smaller cross sections. The cross sections plotted in Fig. 13 are for a limited mass range (i.e., $20\le A\le28$), and hence represent some fraction of the total fusion-fission cross section. Since a folding angle measurement was not performed, the present results do not provide information regarding the fraction of the cross section binary breakup which is consistent with complete fusion.

IV. INTERPRETATION OF THE EVAPORATION RESIDUES

The behavior of the extracted evaporation-residue-like yields can be summarized as follows: (i) the velocity spectra $[(1/v^2)d^2\sigma/d\Omega dv]$ for the heavier evaporation-residue masses (whose identification is subject to little ambiguity) are consistent with a Gaussian shape, (ii) for lighter evaporation-residue masses this is also approximately true, although contributions from other reaction processes become more evident, (iii) for all masses, the
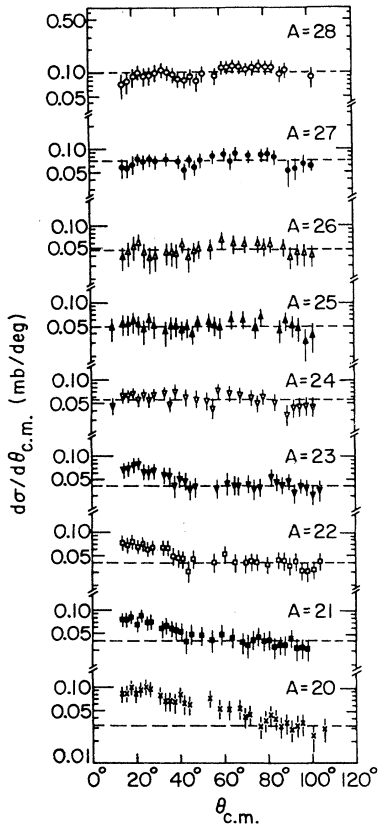

FIG. 12. Angular distributions of the binary fragments in the center-of-mass system for the masses indicated. The horizontal dashed lines have been used to obtain the fusion-fission cross sections.
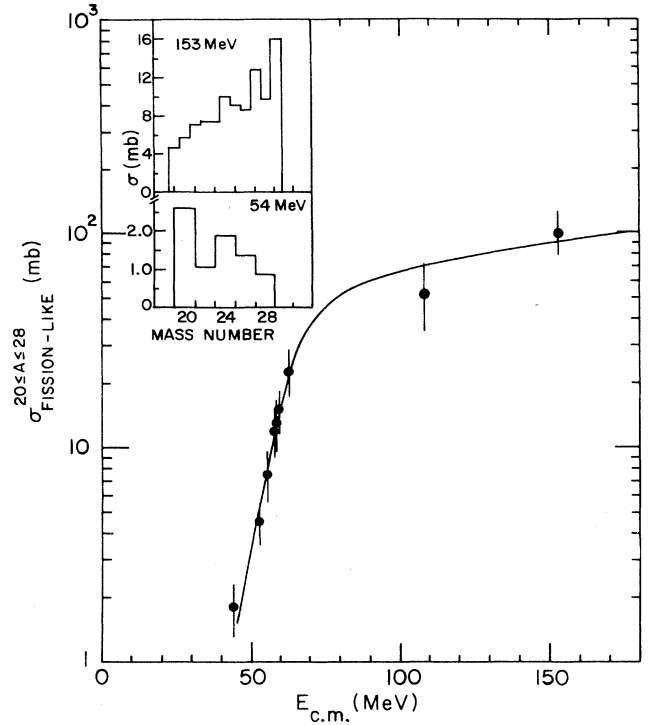
centroids and widths of the velocity spectra are in disagreement with the values predicted by Monte Carlo evaporation codes (i.e., the observed centroids are at a lower velocity than expected and the observed widths are larger than predicted), and (iv) the extracted angular distributions for the evaporation-residue yields (identified by their Gaussian shapes) are found to be significantly broader than predicted.

In this section the detailed mass and angle dependence of the evaporation-residue velocity spectra will be investigated. The analysis given here compares the behaviors observed and predicted for complete fusion in order to highlight apparent discrepancies and to establish, within this framework, cross section limits. In order to have an indication of the uncertainties in the calculations, the behaviors predicted for complete fusion by two Monte Carlo codes were studied and compared.

A. Expected behavior for complete fusion

An expression for the differential cross section for evaporation residues in the laboratory system can be derived in the framework of the simplest picture of the fusion-evaporation process. Assuming (i) that the target and projectile nuclei fuse to form a compound nucleus, (ii) that the light evaporated particles have Maxwellian velocity distributions, and (iii) that the evaporation particles are emitted isotropically in the compound-nucleus moving frame, the following expression can be derived:[16]

$$\frac{d^2\sigma}{dv_{ER}d\Omega_{lab}}$$

$$=Nv_{ER}^2$$

$$\times \exp\left\{-\left[\frac{(v_{ER}-v_{c.m.}\cos\theta_{lab})^2+(v_{c.m.}\sin\theta_{lab})^2}{2s_{ER}^2}\right]\right\},$$

$$(1)$$

where $v_{c.m.}$ and v_{ER} are the velocities of the compound nucleus (velocity of the center of mass) and the evaporation residue, respectively. N is an overall normalization constant, and s_{ER} is the standard deviation of the recoil velocity of the distribution reflecting the details of the deexcitation process. The Galilean-invariant cross section in the laboratory system $[(1/v^2)d^2\sigma/dvd\Omega]$ is a Gaussian shaped distribution centered at $v_{c.m.}\cos\theta_{lab}$ with a magnitude varying as $\exp(-\sin^2\theta_{lab})$ with angle.

The simplifying assumptions made in deriving Eq. (1) are not expected to be fully valid in the reaction being studied. Calculations were performed using the Monte Carlo statistical evaporation codes LILITA[20] and PACE[32] for the velocity spectra and angular distributions of evaporation residues resulting from complete fusion with subsequent light-particle emissions (n,p, and α) for the ^{16}O+^{40}Ca reactions at $E_{lab}(^{16}$O$)=214$ MeV [with $\sigma_{ER}\simeq700$ mb; corresponding to $E^*(^{56}$Ni$)=166.5$ MeV and $J_{max}\simeq42$ $\hbar$]. Calculations were performed first requiring isotropic emission and then allowing anisotropic emission (i.e., where angular-momentum effects are included in the PACE and LILITA simulations). Shown in Fig. 14 are PACE predictions for the evaporation-residue

($32 \leq A \leq 52$) angular distributions in the center of mass for the two cases considered (i.e., forced isotropy and angular momentum induced anisotropy), as well as the behavior of their associated Galilean-invariant cross section centroids as a function of the laboratory angle. For both isotropic and anisotropic light-particle emission the Galilean-invariant cross sections were found to be consistent with a Gaussian shape, but for anisotropic emission the centroids are found to deviate from a $v_{c.m.}\cos\theta_{lab}$ behavior at large angles ($\theta_{lab}>10°$). The magnitude of the departure from $v_{c.m.}\cos\theta_{lab}$ is predicted to increase with the number of nucleons evaporated. This is illustrated in Fig. 15, where the predictions of LILITA are shown. (PACE gives similar results.) For $A=48$ little evidence is seen for a departure from a $v_{c.m.}\cos\theta_{lab}$ dependence, but for $A=36$ a discrepancy of 7–8% is indicated at $\theta_{lab}=30°$. The departures from $v_{c.m.}\cos\theta_{lab}$ for the evaporation-residue masses shown in Fig. 15 were fit assuming the functional form:

$$\frac{v^{centroid}}{v_{c.m.}\cos\theta_{lab}}=a+b\sin^2\theta_{lab}.$$

$$(2)$$

The result of these fits are indicated by the solid curves in Fig. 15. The predicted mass dependence of the velocity deviation can be well reproduced assuming a smooth mass dependence of the coefficient b of Eq. (2). The dot-
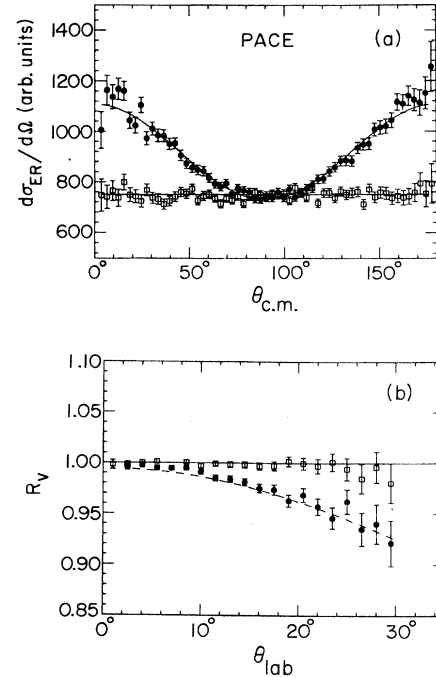
FIG. 14. (a) Center-of-mass angular distributions of the evaporation residues $32 < A < 52$ predicted by PACE for the case of isotropic emission (open squares) and anisotropic emission (solid circles) of light particles. The solid line is a fit of the anisotropy using a Legendre Polynominal of second order (i.e., $d\sigma/d\Omega = A+BP_2[\cos(\theta_{c.m.})]$, with $B/A=0.342$). (b) The laboratory angle dependences of the velocity-deficit ratio R_v for these residues. The anisotropic emission results in deviations of the centroid velocities from a $v_{c.m.}\cos\theta_{lab}$ behavior at larger angles.

ted curves in Fig. 15 are generated with this parametrization using a quadratic mass dependence for the b coefficient.

The effect of anisotropic light-particle emission on the evaporation-residue velocity distribution has been previously addressed in the literature.[33] In a study of the ^{20}Ne$+^{27}$Al reaction, Morgenstern, *et al.*[33] established a semiempirical basis for spectrum decomposition where an assumed $1/\sin\theta_{c.m.}$ angular distribution in the center-of-mass frame reproduced the observed velocity-distribution behaviors. This results in an expression for the evaporation-residue velocity distributions which deviates from a Gaussian and shifts the centroid from a $v_{c.m.}\cos\theta_{lab}$ dependence. In our calculations the evaporation-residue angular distributions in the compound-nucleus frame were found to be well represented by a Legendre polynomial of second order superimposed on an isotropic background [as in Fig. 14(a)]. A pure $1/\sin\theta_{c.m.}$ distribution does not provide a good description of the Monte Carlo simulations.

The widths of the velocity spectra, the shapes of the evaporation-residue angular distributions, and the overall mass distributions predicted by the two codes were also compared. The widths predicted by PACE and LILITA showed the same basic trend. They agreed to better than 20% with PACE predicting, in most cases, about 10% smaller widths than LILITA. The calculated angular distributions were also in basic agreement, with PACE predicting somewhat narrower distributions. The overall mass distributions predicted by the two codes differed appreciably, however, with LILITA predicting the evaporation of approximately 1.5 more nucleons on the average (i.e., $\langle n_{LILITA}\rangle=15.7$ nucleons and $\langle n_{PACE}\rangle=14.2$ nucleons), and significantly different cross sections for specific masses than those predicted by PACE.

From these comparisons it was concluded that: (1) The anisotropic emission of evaporated particles produces evaporation residues whose Galilean-invariant cross sections are Gaussian in shape, but with centroids which deviate from the $v_{c.m.}\cos\theta_{lab}$ behavior of Eq. (1). (2) The kinematic properties of the evaporation residues (i.e., the centroids and widths of the velocity spectra, and the angular distributions) calculated by the two codes are in basic agreement, although with somewhat different mass distributions. The discussion will now focus on the use of these kinematic properties to identify the extract yields consistent with a complete fusion reaction.

B. Decomposition of evaporation-residue yields

1. Single-source decomposition

The relative cross sections at each angle for incomplete and complete fusion were first deduced by comparing the evaporation-residue velocity spectra with LILITA and PACE predictions. The Galilean-invariant cross sections were fit with the maximum complete-fusion component consistent with the data by assuming a Gaussian shaped distribution with the width and peak position fixed at the values predicted by LILITA (PACE), allowing only the height to be a free parameter (as illustrated in Fig. 16). Subtraction of the calculated velocity distribution from the experimental one results in a component centered at lower velocity which for the heavier masses ($A \geq 39$) might be identified as the incomplete-fusion yield, but for the lighter masses also includes yields from binary processes. No evidence of a higher velocity component, corresponding to preequilibrium emission from ^{40}Ca, was apparent in the data. Only about two thirds of the observed residue yields are found to be consistent with complete fusion. The sensitivity of the shapes of the predicted velocity spectra to the cross section assumed in the calculations (taking $\sigma_{ER}=475$ mb and 750 mb) was investigated and found to be small: the ratios of incomplete to complete fusion deduced were essentially the same. The ratio of the complete-fusion cross section σ_{CF} to the total com-
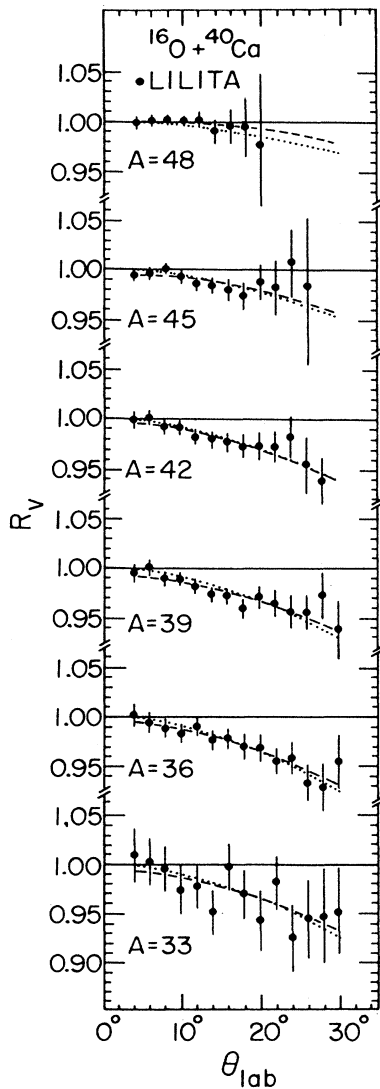

FIG. 15. Predicted angle dependence of the velocity-deficit R_v for representative evaporation-residue masses. The dashed curve is $\sin^2\theta_{lab}$ fit for each mass (see text). The dotted curve is a fit using a smooth quadratic mass dependence for the coefficient b in Eq. (2) (see text).

plete plus incomplete-fusion cross section, $\sigma_{CF} + \sigma_{ICF}$, decreases from 70.9% at 4°, to 61.7% at 28°.

Angular distributions were extracted for the yields identified as consistent with complete fusion for $32 \leq A \leq 50$. The angular distributions extracted for $A = 37, 40, 43,$ and 46 are shown in Fig. 17. The solid curves are the complete-fusion angular distributions predicted by LILITA and normalized to the data at forward angles. The measured angular distributions are significantly broader and peak at a larger angle than predicted by LILITA, especially for the lighter mass residues. The angle integrated complete fusion mass distribution, $\sigma_{ER}^{CF}(A)$, derived using the above procedure based on velocity spectra is compared in Fig. 18 with the total evaporation-residue cross section discussed in the previous section. The integrated mass distribution gives a cross section of $\sigma_{ER}^{CF} = 528 \pm 100$ mb. The σ_{ER}^{CF} cross sec-

tions for individual masses are tabulated in Table I. A similar cross section is obtained if one performs the decomposition using the mass-summed $(32 \geq A \geq 50)$ velocity spectra, where a total cross section of 558 ± 100 mb is obtained. The angular distribution extracted from the mass-summed velocity spectrum is shown in the lower frame of Fig. 17, compared to that extracted for the total yields identified as evaporation residues (Sec. III).

The mass distribution obtained in the decomposition implies that the average number of evaporated nucleons is larger $(\Delta n \simeq 2$ nucleons$)$ than predicted for complete fusion. Possible explanations for this result and discrepancies noted previously regarding the broader angular distributions, fall into two general categories; (1)
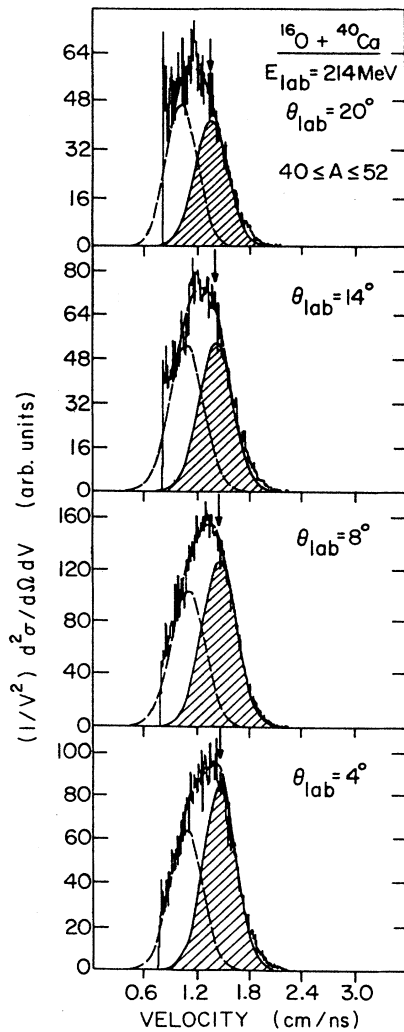
FIG. 16. Relative contributions of complete fusion (hatched distribution calculated by LILITA) and incomplete fusion (open Gaussian) to the summed $(40 < A < 52)$ velocity spectra observed at the indicated laboratory angles. The arrows indicate the expected velocity for full linear-momentum transfer.
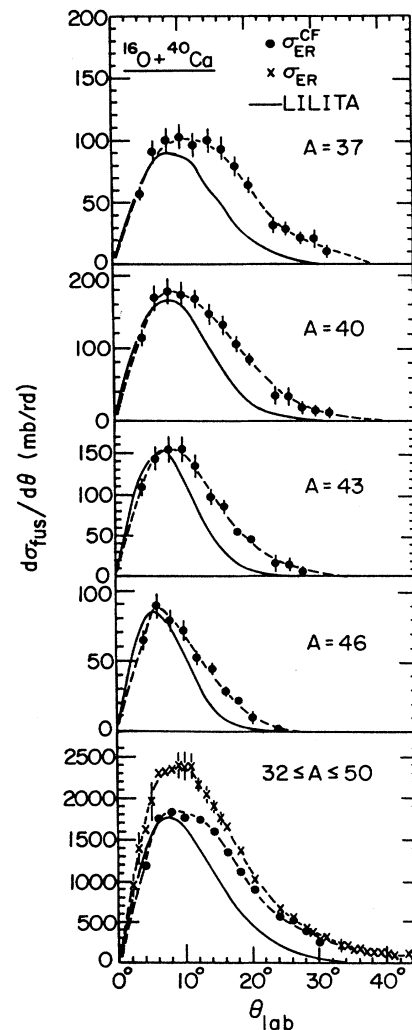
FIG. 17. The angular distributions of evaporation-residue yields consistent with full linear-momentum-transfer (complete fusion) for representative masses and for the summed masses $(32 \leq A \leq 50)$ are indicated by the solid circles (the dashed lines are to guide the eye). The solid lines are LILITA predictions normalized to the most forward angles data points. The angular distribution for the total evaporation-residue yields is indicated by the crosses.

FIG. 18. The complete-fusion evaporation-residue mass distribution extracted using predicted velocity distributions (solid histograms) is compared to the mass distribution extracted for all evaporation residues.

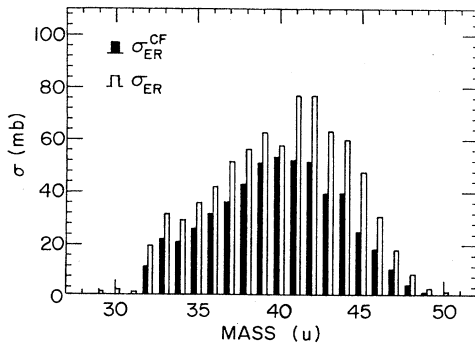the evaporation codes are inadequate in some way (e.g., the input parameters are incorrect, or important decay channels have not been included), or (2) preequilibrium particle-emission processes play an important role. Both explanations are reviewed in the following sections: the role of preequilibrium emission is investigated in the next section, and the possible inadequacies of the evaporation code calculations will be discussed in Sec. IV C.

2. Two-source fits

Based on the single-source decomposition of velocity spectra, a maximum of two thirds of the evaporation-

TABLE I. Experimental cross sections

A	$\sigma_{\text{Total}}^{a}$ (mb)	σ_{ER}^{b} (mb)	σ_{ER}^{c} (mb)
29	23.8	0.9	
30	25.5	2.1	
31	30.1	7.0	
32	37.6	18.9	11.0
33	48.6	31.2	21.6
34	42.0	28.7	20.5
35	49.9	35.3	25.6
36	62.9	41.6	31.1
37	70.9	51.0	35.6
38	74.6	55.6	42.4
39	82.4	62.2	50.4
40	70.0	57.0	52.8
41	90.3	76.5	51.5
42	93.6	76.2	51.0
43	71.5	62.7	38.8
44	64.7	59.5	39.2
45	46.7	46.7	24.0
46	30.3	30.3	17.6
47	17.5	17.5	9.9
48	8.1	8.1	3.7
49	2.5	2.5	1.0
50	1.1	1.1	

aTotal yield observed for mass group.
bYield identified as evaporation-residue-like (see Sec. III).
cYield identified as consistent with complete fusion based on predicted velocity distributions (see Sec. IV B 1).

residue yield is consistent with full linear-momentum transfer. The centroid of the incomplete-fusion yield is consistent with what is expected from a reaction process in which a preequilibrium alpha particle is emitted at roughly beam velocity in the beam direction. This incomplete-fusion channel [$^{16}\text{O} + {}^{40}\text{Ca} \rightarrow ({}^{12}\text{C} + {}^{40}\text{Ca}) + \alpha$] was used in our initial two-source simulation of the evaporation-residue behavior.

PACE calculations were performed for $^{16}\text{O} + {}^{40}\text{Ca}$ (the ^{16}O source) at $E_{\text{lab}} = 214$ MeV (13.4 MeV/nucleon) with $\sigma_{\text{ER}} = 660$ mb, and $^{12}\text{C} + {}^{40}\text{Ca}$ (the ^{12}C source) at $E_{\text{lab}} = 160.5$ MeV (13.4 MeV/nucleon) with $\sigma_{\text{ER}} = 540$ mb. These cross sections correspond to approximately equal maximum impact parameter for the two reactions. Combining the velocity spectra predicted for the same residue mass from the two reaction processes results in a Gaussian-shaped velocity distribution with one centroid shifted with respect to full linear-momentum transfer. The behavior of these new velocity distributions was compared to the observed distributions. The ratio for the probability of incomplete to complete fusion was adjusted to best reproduce the observed angle dependences of the velocity centroids (Figs. 5 and 6). With cross section weightings of 0.60 ($\sigma_{\text{ER}} = 454$ mb) and 0.40 ($\sigma_{\text{ER}} = 298$ mb) for the ^{16}O and ^{12}C sources, respectively, good descriptions of the velocity deficits for the lighter masses (e.g., $A < 45$; see Fig. 5) are obtained, but the calculations fail to reproduce the observed deficits for the heavier masses ($A > 45$). As will be discussed below, these calculations also do not reproduce the observed velocity-distribution widths.

The predicted angular distributions are in better agreement with extracted differential cross sections, but the falloff at larger angles is still not reproduced. In Fig. 19 the extracted mass-summed angular distribution is compared with the prediction; the ^{12}C source alone is in
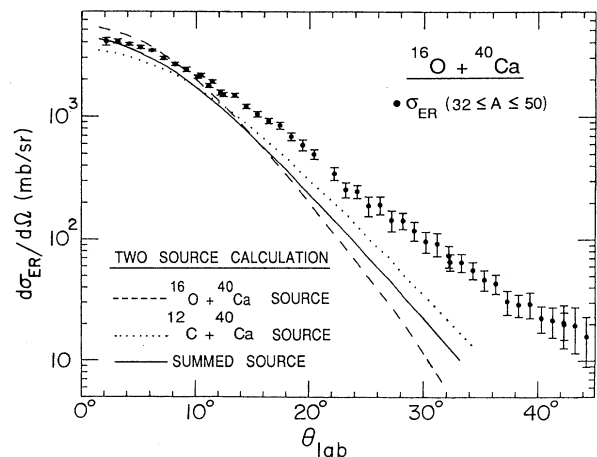

FIG. 19. Angular distribution of the yields identified as evaporation residues (solid circles). The solid curve is the PACE predicted angular distribution from the two-source simulation. The dashed and dotted curves are the predicted angular distributions for the complete-fusion and incomplete-fusion sources which have arbitrarily normalized for comparison of the shapes. (See text.)

better agreement. The predicted mass distribution of this two-source simulation is compared in Fig. 20 with the mass distribution observed for evaporation residues. The ^{12}C mass distribution can be seen to peak at lower masses than the ^{16}O mass distribution with no yields predicted for $A_{ER} > 46$. Certain masses (e.g., $A = 37$, and 43) are underpredicted when compared to their neighbors, raising questions regarding the limitations of PACE (or any presently available evaporation code) for predicting the details of evaporation at these high excitation energies. Compared to the predicted complete-fusion (^{16}O source) mass distribution alone, the summed-source distribution is in significantly better agreement with the extracted evaporation-residue distribution.

The predicted trend of the velocity deficits for the lighter masses (Fig. 5) can be seen from our simulation to depend on the details of the sources involved. For $A = 45$ there is a predicted trend to smaller momentum deficit with increasing angle, which is consistent with the data. On the other hand, the predictions for $A = 39$ and 42 have trends of increasing linear-momentum-transfer deficit with increasing angle. This is not evident in the mass 42 data, but is consistent with the mass 39 data. The predicted mass and angle dependence of the linear-momentum-transfer deficits is sensitive not only to the ratio of the strengths of the sources, but also to what sources are involved since the sources will have different

FIG. 20. In the upper frame the predicted mass distribution from the two-source simulation is compared to the extracted evaporation-residue mass distribution (solid histograms). In the lower frame the relative intensities of the predicted complete- and incomplete-fusion mass distributions are compared.

initial recoil velocities and different evaporation sequences. The angle dependence of the velocity deficits for evaporation residues with contributions from incomplete fusion has been discussed by Pochodzalla, et al.[34] who pointed out that this angle dependence must be taken into account before drawing any conclusions about the linear-momentum transfer. In their treatment the observed velocity-deficit behavior is interpreted in terms of a single anisotropic source. While this procedure would appear to be useful for the extraction of the mean-evaporation-residue deficit at 0°, our two-source simulations indicate that the velocity-deficit behavior depends on the velocity and decay properties of the sources contributing, and a single-anisotropic-source parametrization would not be capable of reproducing the detailed behavior.

The assumption that preequilibrium alpha particles are emitted at beam velocity in the beam direction is clearly an oversimplification. Emission of alpha particles at higher energies will produce incomplete fusion compound nuclei at correspondingly lower excitation energies, moving at a slower velocity in the laboratory system. This might explain the failure of our two-source simulation to reproduce the observed deficits for masses $A > 45$. To test this, PACE calculations were performed for two such sources [$E_{lab}(\alpha)=108$ and 162 MeV]. Using these sources to reproduce the $A = 49$ results was found to seriously worsen the fit to the linear-momentum-transfer values for the other masses. In the framework of the evaporation codes and parameters used, the heavy-mass linear-momentum-transfer deficits cannot be explained solely on the basis of a ^{12}C incomplete-fusion source.

To study the influence of the assumption of 0° preequilibrium alpha emission on the predicted evaporation-residue angular distributions, a two-source model simulation was performed assuming preequilibrium emission of 54 MeV (13.4 MeV/nucleon) alpha particles with a Gaussian angular distribution peaked mean at the grazing angle ($\theta_{lab}=6°$) and width (FWHM) of 15°. This trial distribution results in an increase of less than 10% in the residue differential cross section at large angles, and thus there still remains a serious difficulty in reproducing the experimentally-measured, evaporation-residue differential cross sections. Similarly, the widths of the velocity distributions are only increased by $\approx 10\%$ and are still significantly narrower than observed (Fig. 7).

3. Three- and four-source fits

Because of the inability to explain the heavy mass ($A > 45$) linear-momentum-transfer deficits using the ^{12}C incomplete-fusion source, other possible sources for the production of these residues were considered. The results of several multi-source simulations can be summarized as follows: (i) Preequilibrium single- or two-nucleon emission sources do produce heavy evaporation-residue masses ($A > 45$) with significant cross section; but if the nucleon(s) is (are) emitted at beam velocity ($E_{lab}=13.4$ and 26.8 MeV for the one- and two-nucleon emission, respectively), insufficient linear momentum is carried away to account for the velocity deficits. (ii) The observed be-
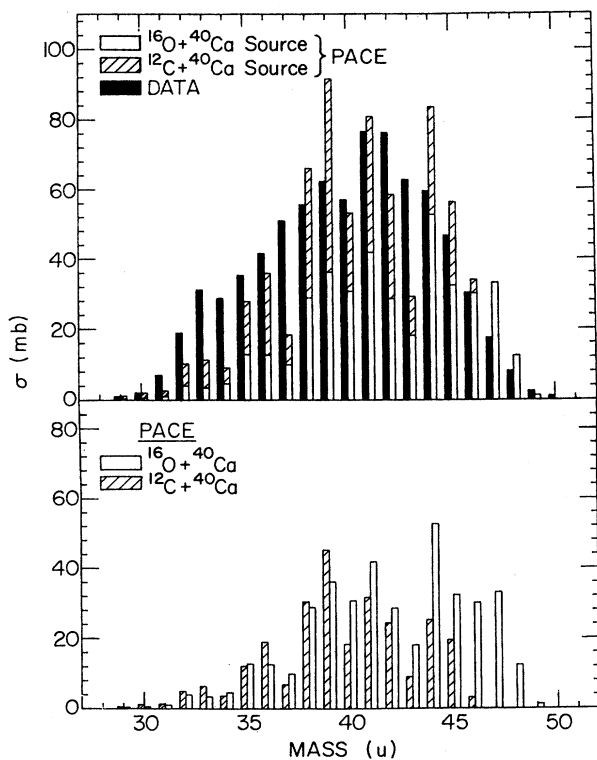
havior of the velocity centroids for the heavier masses can be reproduced using ^{15}N and/or ^{14}N sources assuming preequilibrium emission of protons at $E_{lab} = 34$ or 50 MeV and deuterons at $E_{lab} = 26$ or 34 MeV (with appropriately adjusted probabilities for ^{16}O and ^{12}C sources). In Fig. 5 the dashed curves represent the predicted velocity centroids for the various masses in a three-source simulation with source weights of 0.60 ($\sigma_{ER} = 456$ mb), 0.30 ($\sigma_{ER} = 228$ mb), and 0.10 ($\sigma_{ER} = 76$ mb) for the ^{16}O, ^{12}C, and ^{15}N sources, respectively. In this simulation the ^{15}N source was assumed to be the compound nucleus formed (^{15}N + ^{40}Ca → ^{55}Co) after the emission of a 50 MeV proton at $0°$. Although these multi-source simulations did reproduce the observed evaporation-residue mass distribution rather well, the predicted angular distributions were still narrower than observed.

Without inclusion of realistic energy and angular distributions for the preequilibrium single- and two-nucleon emission, the predictions of multi-source simulations cannot be used to draw conclusions. It is clear, however, that if single- and two-nucleon preequilibrium emission occurs (as appears to be indicated) a proper treatment of energy spectra for the preequilibrium emission will lead to a significant decrease in the cross section which has been identified with complete fusion.

C. Further discussion of evaporation models

There are three major areas of disagreement between our data and the predictions of complete-fusion evaporation calculations: (a) the linear-momentum-transfer deficits, (b) the broadened evaporation-residue angular distributions and velocity-distribution widths, and (c) the shifted evaporation-residue mass spectrum. The linear-momentum deficits require the presence of one or more incomplete-fusion processes. The extent to which the other observed differences between experiment and theory can be attributed entirely, or even partially, to incomplete-fusion processes is not clear. The various complete/incomplete source simulations were unable to increase significantly either the widths of the velocity distributions or the angular distributions for the lighter evaporation-residue masses. This would suggest that the evaporation calculations should be looked at more closely.

Although a detailed investigation of the possible inadequacies of the evaporation codes used was not performed, some of the more obvious questions regarding the uncertainties of these calculations were explored, namely: (1) the choice of level-density parameters, (2) the role of discrete levels, (3) the role of heavier-particle decay, and (4) the influence of compound-nucleus deformation on the decay probabilities, energy spectra, and angular distributions of the evaporated particles.

The PACE and LILITA programs assume a constant level-density parameter, "a," throughout the evaporation cascade ($a = 8.5$ for the PACE and 7.5 for LILITA calculations discussed). The sensitivity of the results to this parameter was explored by comparing PACE calculations with $a = 7.0$, 8.5, and 10.0. For the higher density-

parameter values the predicted mass distribution is shifted to somewhat lower values, but in each of these calculations the highest masses ($A > 45$) remain substantially overpredicted and the lower masses underpredicted. Variations in the choice of the density parameter, while important for individual mass predictions at the 10% level, cannot readily account for the general features of our data.

In the PACE code the excitation energy and spin of known levels in the residue nuclei can be incorporated. Calculations were performed with all known levels (> 3400) of the residue isotopes $32 < A < 49$. These calculations produced a somewhat altered mass distribution which is in only slightly better agreement with the observed mass distribution. In particular some of the mass anomalies discussed above are less apparent, although still visible. Interestingly enough, the most pronounced effect of using discrete levels is not directly visible in our data: the Z distribution of residues for a given mass becomes appreciably narrower for most of the residue masses. Future experiments with both A and Z identification should be able to verify if this concentration occurs.

Neither PACE or LILITA evaporation codes had provisions for heavier-particle ($Z > 2$) evaporation during the cascade. While the deexcitation of the ^{56}Ni compound system proceeds predominantly via light particle emission (neutron, proton and alpha) at relatively low excitation energies, at E^* (^{56}Ni) $= 166.5$ MeV the heated composite system can conceivably emit more complex clusters[35-38] (e.g., Li, Be, B and C). Heavier-particle evaporation would naturally lead to broader angular distributions and an increased population of lower mass residues. Both of these features are present in our extracted yields. Since the angular-momentum-induced evaporation anisotropy is more prevalent for heavier evaporated masses, a larger deviation of R_v from Eq. (1) would be expected for complete-fusion evaporation residues than predicted by our calculations. If this is the case, our present analysis would underestimate these complete-fusion cross sections. While such heavier particle evaporation would not appear to be responsible for all of the disagreements between calculation and experiment found here, its presence would explain some of the more glaring discrepancies. The observations of asymmetric mass distributions for fission fragments observed in reactions forming compound nuclei ($A \leq 100$) below the Businaro-Gallone point[39] provide evidence that heavy-particle evaporation or very mass-asymmetric fission should be present at some level. In particular the results of Sanders *et al.*[22] for the ^{16}O + ^{40}Ca reaction at lower bombarding energies support this conjecture. The question of heavier-particle evaporation can only be directly addressed with coincidence data.

The potential importance of deformation effects in this mass region has been discussed in the literature. Blann[40,41] has investigated the consequences of large nuclear deformation on the deexcitation process. Furthermore Dichter *et al.*[42] have found some indications of the existence of shape isomers in ^{56}Ni, in qualitative agreement with a prolate superdeformation at high angular

momenta.[41] The deformed ^{56}Ni calculations of Ref. 41 predicted more energetic alpha decay as well as enhanced ^{8}Be emission-producing evaporation residues with broadened angular distributions. The influence of such deformation effects on the decay channel competition and on the detailed energy spectra of the emtited particles could also be responsible for some of the discrepancies discussed here.

D. Summary

In the single-source decomposition, maximum yields consistent with the predicted evaporation-residues velocity distributions were extracted. An upper limit for the complete fusion evaporation-residue cross section of $\sigma_{CF}=528\pm100$ mb (Sec. IV B 1) was established. In the two- and multi-source decompositions, the velocity centroid behaviors of the various evaporation-residue masses as a function of angle were used to determine the relative probability of the complete and incomplete source(s). Maximum complete-fusion evaporation-residue cross sections of 494 mb and 400–450 mb were extracted. Based on these analyses we deduce an upper limit on the complete-fusion evaporation-residue cross section of $\sigma_{CF}=475\pm100$ mb.

The procedures used to extract the complete-fusion evaporation-residue cross section are reasonable to the extent that the evaporation codes predict the decay of the complete-fusion compound nucleus rather well. The possible inadequacies and uncertainties of the evaporation calculations (discussed in the previous section) limit the conclusions that can be drawn and prevent the placement of better limits on the complete-fusion cross sections. Nevertheless, a number of observations can be made: (i) The discrepancies between the extracted evaporation-residue angular distribution, velocity-distribution widths, the angle integrated mass distribution and the predicted behaviors strongly suggest that heavier-particle evaporation occurs; (ii) the two-(multi) source simulations show that the kinematic properties of the evaporation residues (i.e., the velocity centroids and widths, and angular distributions) are sensitive to the character and relative magnitudes of the sources contributing. Our model simulations indicate that 30–40% of the evaporation-residue yields arise from preequilibrium alpha-particle emission and > 10% from the single- or two-nucleon emission. A more realistic treatment for preequilibrium single-nucleon emission reaction component, in particular, would be expected to reduce the identified complete-fusion fraction significantly.

V. DISCUSSION

A. Linear-momentum transfer

The average velocity-deficit ratio ($\langle R_v \rangle = 0.885 \pm 0.020$) observed in the present study is in agreement with that reported by Chan et al.[1] for the ^{16}O$+^{40}$Ca reaction at a bombarding energy of 13.6 MeV/nucleon, and with the systematics for the energy dependence of $\langle R_v \rangle$ established in studies of light-heavy-ion projectiles on a

variety of target nuclei. Using the value of 475 mb for the complete-fusion evaporation-residue cross section, the fraction of complete fusion to total evaporation-residue cross section, R_σ [$\sigma_{CF}/(\sigma_{CF}+\sigma_{ICF})$], observed is 0.63 ± 0.10. This fraction is in good agreement with the systematic behavior observed by Morgenstern et al.[43] Morgenstern's analysis showed that for different reactions, at the same relative velocity, incomplete fusion is more likely to appear for a mass-asymmetric entrance channel than for a symmetric one. Their results were plotted as a function of the velocity of the light-reaction partner with respect to the center of the mass; i.e.,

$$v_L = \frac{A_H}{A_H+A_L} v_{rel} \quad (3)$$

where A_L and A_H are the masses of the light- and heavy-reaction partners respectively. The relative velocity, v_{rel}, is defined as:

$$v_{rel} = \left[\frac{2(E_{c.m.}-V_{coul})}{\mu} \right]^{1/2} \quad (4)$$

where $E_{c.m.}$ and V_{coul} are the center-of-mass kinetic and Coulomb energies, respectively, and μ is the reduced mass. These results, together with the complete-fusion fraction obtained in the present study [$v_L/c=0.1098$, $A_H/(A_H+A_L)=0.714$, and $v_{rel}/c=0.1537$], are shown in Fig. 21. The common onset for incomplete fusion and the disappearance of complete fusion implied by the results when plotted as a function of v_L are argued to indicate that incomplete-fusion processes are associated with those reactions where the vector coupling of the Fermi motion of individual nucleons (in the projectile and target) with the relative motion of the interacting nuclei produce nucleons with sufficient velocities to escape.

The number of preequilibrium emitted nucleons N_{em} responsible for the observed evaporation-residue velocity centroids can be estimated[44] under the assumption that
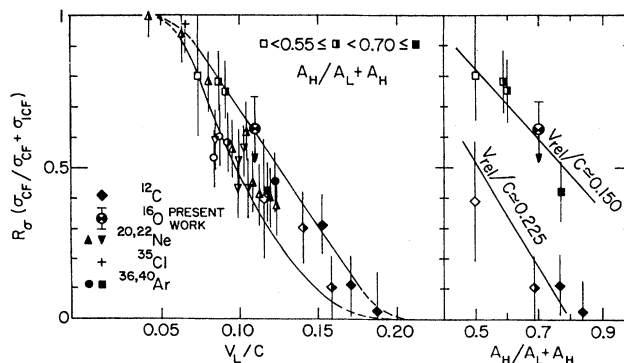

FIG. 21. Figure from Ref. 43 displaying on the left-hand portion the fraction of complete fusion as function of the velocity of the lighter nucleus v_L/c, and on the right-hand portion the fraction of complete fusion for various reactions at the same relative velocity as function of the entrance channel mass asymmetry $(AH/AH + AL)$. (See text.) The symbols represent data from Ref. 43 except for the large symbols which indicate the result of the present work.

the escaping nucleons have the same velocity along the beam axis; i.e.,

$$A_{\mathrm{p}} v_{\mathrm{p}} = [A_{\mathrm{p}} + A_{\mathrm{t}} - N_{\mathrm{em}}] v_{\mathrm{er}} + N_{\mathrm{em}} v_{\mathrm{em}} \qquad (5)$$

where the subscripts p, t, er, and em refer to the projectile, the target, the detected evaporation residue, and the emitted nucleons, respectively. Assuming that the nucleons escape with the velocity of the projectile, the effective mass necessary to impart the linear momentum implied by the observed velocity centroid can be evaluated. The difference in the number of nucleons of the projectile and the effective projectile, N_{em}, can be expressed as a function of average velocity-deficit ratio $\langle R_v \rangle$:

$$N_{\mathrm{em}} = A_{\mathrm{p}} - \frac{A_{\mathrm{t}} \langle R_v \rangle}{\left[\dfrac{(A_{\mathrm{p}} + A_{\mathrm{t}})}{A_{\mathrm{p}}} - \langle R_v \rangle \right]} \qquad (6)$$

The ratio $\langle R_v \rangle$ of 0.885 observed in the present study implies that approximately 2.5 nucleons have been emitted from the ^{16}O projectile before amalgamation with the target, in agreement with the systematics of Stephans *et al.*[44] The observation by Budzanowski *et al.*[45] that on the average only half of the ^{16}O projectile is captured by the ^{40}Ca target at $E_{\mathrm{lab}} = 20$ MeV/nucleon is also consistent with these systematics. In Fig. 22 the evaluated N_{em} for each mass group is plotted as a function of the total missing mass ($A_{\mathrm{CN}} - A_{\mathrm{ER}}$), showing a trend which is similar to that reported for reactions on similar systems.[1,19,21,46] A larger number of preequilibrium nucleons is associated with the lighter evaporation residues.

Based on the results of our two-source simulation there are two observations regarding the N_{em} behavior which can be made. First, the observed N_{em} trend in Fig. 22 can be understood as resulting from the varying contributions of the complete- and incomplete-fusion sources to the evaporation-residue mass groups. Second, because of the kinematics and decay characteristics of the sources and the assumption that all emitted particles are at beam velocity, the extracted N_{em} represent only approximate
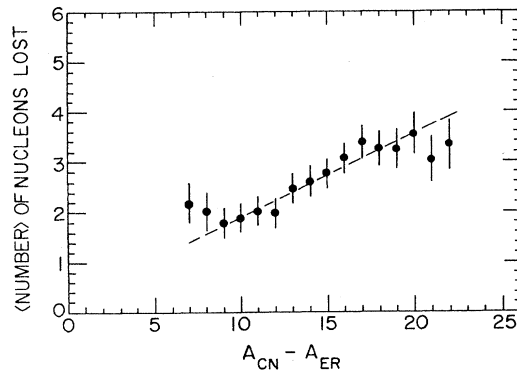

FIG. 22. Average number of nucleons lost by the projectile deduced from the velocity-deficit fraction R_v exhibited by each evaporation-residue mass group plotted as a function of the total missing mass ($A_{\mathrm{CN}} - A_{\mathrm{ER}}$). The dashed line is a guide to the eye.

estimates of the actual number of emitted nucleons. Our two-source simulation fits to the observed velocity deficits (which take into account the different velocity and angular distributions of the evaporation residues from the two sources) indicate that on the average only 1.6 nucleons are emitted, compared to the 2.5 nucleons obtained using Eq. (6). Inclusion of substantial single- and/or two-nucleon emission sources would lead to better agreement with the value from N_{em} of Eq. (6). However, the observed sensitivity of $\langle R_v \rangle$ to the details of the contributing velocity distributions suggests that the physical significance of the extracted N_{em} should be viewed with caution.

Although the average number of lost nucleons obtained from the velocity-deficit ratios is found to follow the systematics based on the simple picture of overlapping Fermi spheres as parametrized by Stephans *et al.*,[44] Fermi-jet calculations[47,48] account for only a small fraction of the number of nucleons emitted. The precompound decay calculations of Blann[49,50] appear to have better success in predicting the energy dependence of $\langle R_v \rangle$. Our calculations with the Blann BME model predict a momentum deficit of about 8% compared to the observed 11.5% in our measurements. The origins of incomplete-fusion sources [Fermi-jets, promptly emitted particles (PEP), precompound decays, or massive transfer] are not well understood and are still under theoretical investigation.[51−57] At lower energy (≤ 7 MeV/nucleon) there is evidence[58−61] that the evaporation residues associated with incomplete fusion originate from cluster transfer reactions. At higher bombarding energies results from the SARA and GANIL facilities[3,5,62] indicate that in this energy regime the Fermi motion of the individual nucleons in the interacting nuclei plays a key role. At 13.4 MeV/nucleon the appropriate description is not established. Better information about the energy and angular distributions of the preequilibrium particles emitted is needed.

B. Evaporation-residue cross sections

In comparing the present results with those obtained from previous measurements, it is necessary to consider the uncertainties associated with deriving a complete-fusion evaporation-residue cross section from the data, as discussed in the previous sections. It has already been shown that the present results are consistent with the earlier measurements of Vigdor *et al.*,[7] within statistical and systematic experimental uncertainties. It is now understood, however, that the fusion cross sections quoted in the earlier work included both complete- and incomplete-fusion components as well as some binary reaction yields. The success of the Morgenstern systematics in reproducing the observed complete-fusion fraction at $E_{\mathrm{lab}} = 214$ MeV suggests that these systematics can also be used to deduce this fraction at the lower energies (i.e., 104 and 140 MeV) measured in the work of Vigdor, *et al.*[7] These systematics imply complete-fusion fractions of 0.93, 0.82, and 0.63 at bombarding energies of 104, 140, and 214 MeV, respectively, for the ^{16}O + ^{40}Ca reaction. Cross sections were extracted by using the an-

gular distributions predicted LILITA normalized to the data at forward angles by the Morgenstern complete fusion fraction. This results in maximum possible complete-fusion evaporation-residue cross sections of 1009, 699, and 464 mb, for the three bombarding energies of 104, 140, and 214 MeV, respectively. The cross section of 464 mb obtained from the Vigdor data at 214 MeV is in good agreement with the 475 mb extracted in the present study. The same procedure applied to the mass-summed angular distributions observed in the present study yields a cross section of 440 mb. These extracted maximum values for the evaporation-residue cross sections are shown in Fig. 23 together with the cross section obtained in the present study and those reported at lower bombarding energies.[7,63]

The complete-fusion evaporation-residue cross sections for the ^{16}O+^{40}Ca,[7,63] ^{28}Si+^{28}Si (Refs. 8 and 64) and ^{32}S+^{24}Mg (Refs. 9, 65, and 66) reactions are compared in Fig. 24. The large cross sections at $E_{lab} > 10$ MeV/nucleon for the ^{16}O+^{40}Ca reaction reported by Vigdor, et al.[7] had suggested a strong entrance-channel effect at higher bombarding energies. The present cross section extracted at 214 MeV, together with the estimated evaporation-residue cross sections obtained from reanalysis of the Vigdor data indicate that the ^{16}O+^{40}Ca complete-fusion evaporation-residue cross section energy dependence is quite similar to that exhibited by the ^{28}Si+^{28}Si and ^{32}S+^{24}Mg systems. A common limitation of the evaporation-residue cross section at high incident energy emerges from this comparison. The critical angular momenta deduced from the experimental data for these three systems, using the sharp cutoff approximation, are shown plotted versus the excitation energy in
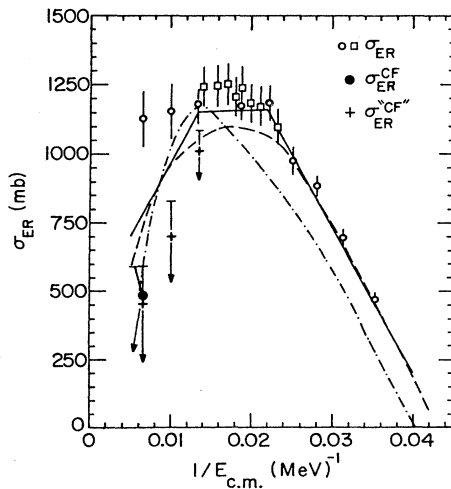

FIG. 24. Complete-fusion evaporation-residue cross sections for ^{16}O+^{40}Ca (Refs. 7, 63, and present work), ^{28}Si+^{28}Si (Refs. 8, 63, and 64), and ^{32}S+^{24}Mg (Refs. 9, 65, and 66) are shown plotted as solid circles, solid triangles, and open squares, respectively, as a function of $Z_1 Z_2 e^2 / E_{c.m.}$.

the compound nucleus, ^{56}Ni, in Fig. 25. The dashed vertical lines correspond to the angular momenta calculated for a vanishing symmetric fission barrier ($B_f = 0$) and a symmetric fission barrier comparable to the nucleon separation energies ($B_f = 8$ MeV), respectively. (The fission barriers were calculated using the macroscopic model of

FIG. 23. Complete-fusion evaporation-residue cross sections for the ^{16}O+^{40}Ca reaction. The data points were taken from Ref. 7 (open circles), Ref. 63 (open rectangles), and this work (solid circle). The plus symbols are upper limits on the cross sections obtained from reanalysis of the data of Ref. 7, as discussed in the text. The dot-dash, dashed, and solid curves represent fusion-model calculations for the total complete-fusion cross section behaviors of Ref. 69, Ref. 70, and Refs. 71, 72, and 26, respectively.
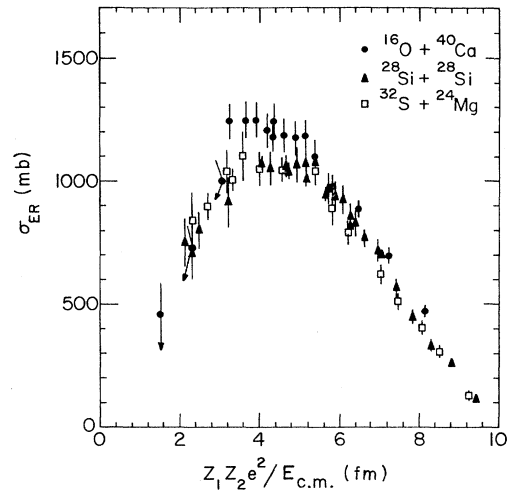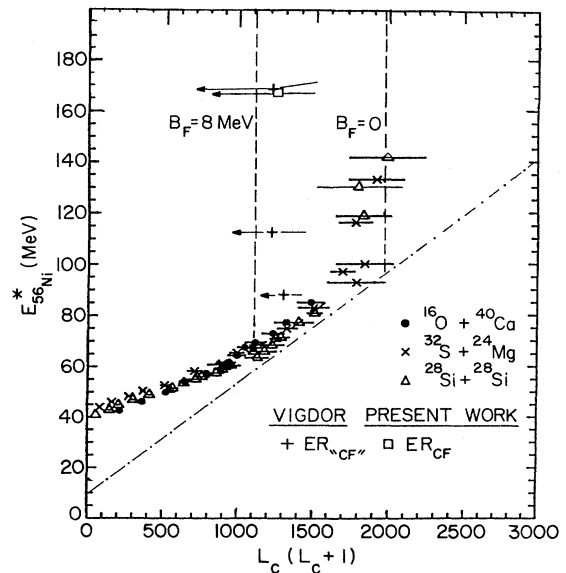

FIG. 25. The critical angular momenta extracted from the complete-fusion evaporation-residue cross sections (Fig. 24) for the three system forming the compound nucleus ^{56}Ni under the assumption of a sharp cutoff partial-wave distribution are plotted as a function of the excitation energy in ^{56}Ni. The dot-dashed line corresponds to the statistical yrast line (Ref. 72), with $\Delta Q = 10$ MeV and $r_0 = 1.20$ fm. The dashed lines indicate the calculated angular momenta for fission barriers of $B_f = 0$ and 8 MeV using the Sierk macroscopic model (Ref. 68).

Sierk,[67,68] which includes diffuse surface and finite nuclear range effects.)

The evaporation-residue angular momenta extracted for the $^{16}O + ^{40}Ca$ system compare rather well with the calculated fission-barrier limits. On the other hand, while a saturation in critical angular momenta for the $^{28}Si + ^{28}Si$ and $^{32}S + ^{24}Mg$ systems is indicated, the extracted critical angular momenta are somewhat larger than expected based on the calculated fission barrier limits. Before drawing any conclusions from these behaviors it is important to establish clearly whether incomplete-fusion contributions of significant magnitude are present in the evaporation-residue yields for the symmetric systems. In contrast to the $^{16}O + ^{40}Ca$ reaction, little evidence for the presence of significant incomplete-fusion contributions has been found for the $^{28}Si + ^{28}Si$ (Ref. 8) and $^{32}S + ^{24}Mg$ (Ref. 9) reactions at comparable bombarding energies. A similar conclusion was reached in a study of the $^{19}F + ^{40}Ca$ and $^{32}S + ^{27}Al$ reactions leading to the ^{59}Cu compound nucleus.[21] Based on the Morgenstern systematics the magnitude of the incomplete-fusion cross sections for these symmetric entrance-channel systems should be significantly smaller than that for the $^{16}O + ^{40}Ca$ system. On the other hand, the results of the $^{19}F + ^{40}Ca$ and $^{32}S + ^{27}Al$ study (Refs. 21 and 34) indicate that the complete-fusion evaporation-residue cross sections which were extracted for the $^{32}S + ^{27}Al$ reaction are consistent with the calculated fission-barrier limits. The authors[34] suggest that the differences observed in the evaporation-residue cross sections for the symmetric and asymmetric systems are a result of the incomplete-fusion contribution appearing in the fission channels for the symmetric systems and the evaporation-residue channel for the asymmetric systems. Further coincidence measurements for the symmetric entrance-channel reactions are needed.

C. Complete-fusion cross sections

The energy dependence of the complete-fusion cross sections for the $^{16}O + ^{40}Ca$ reaction predicted by several fusion models are compared with the extracted upper limits for the complete-fusion evaporation-residues cross sections in Fig. 23. Shown are the complete-fusion cross sections predicted by the one-dimensional Proximity Potential Plus Friction model of Birkelund and Huizenga,[69] the Surface Friction model of Fröbrich,[70] and the "Successive-Critical-Distance" model of Matsuse, *et al.*[26,71,72] All of these models overpredict the experimental complete-fusion evaporation-residue cross sections in the high-energy region (as well as the limiting cross section suggested for the evaporation residues by the Sierk fission barriers). Part of this discrepancy may reflect the fact that fission channels are not included in the experimental cross sections, yet are implicitly included in the model calculations. In the case of the Proximity Plus Friction model, the difference between the predicted total-fusion cross section and observed evaporation-residue complete-fusion cross section is of the order of 100 mb, while in the case of the Surface Friction and "Successive-Critical-Distance" models it is on the order 350 mb.

Information about the total-fission cross section behav-

ior for the $^{16}O + ^{40}Ca$ reaction has only recently become available and is still fragmentary. Measurements for a limited mass range $(20 \le A \le 28)$ reported by Sanders, *et al.*[22] indicate that the cross sections increase from 1 to 20 mb over the energy range $70 \le E_{lab}(^{16}O) \le 90$ MeV. As discussed in Sec. III C, yields consistent with fission over a similar mass range have been extracted in this study, yielding a cross section of 98 ± 10 mb. The limited fusion-fission mass distributions at 214 MeV and at 76.9 MeV (see Fig. 13), suggest a transition from an asymmetric decay to a more symmetric decay of the ^{56}Ni compound nucleus. As discussed by Sanders, *et al.*[22,23,27] the fissility of the ^{56}Ni compound nucleus is below the Businaro-Gallone point[39] and should yield an asymmetric fission mass distribution[35-38,73] at low excitation energies and angular momenta. However, at higher bombarding energies the higher partial waves which participate are expected to be responsible for increased symmetric fission decays.[26] The fission cross section observed in the present study in the mass range $20 \ge A \ge 28$ may be augmented by another ~ 100 mb outside of this range. It is not possible from this study alone to deduce the fraction of fission yields which arise from incomplete fusion. The results of Brzychczyk, *et al.*[28] (also for a limited mass range) for the $^{16}O + ^{40}Ca$ reaction at $E_{lab} = 230$ MeV, indicate that the magnitude of complete fusion-fission yields going to symmetric fission channels is small, although finite, as compared to the incomplete fusion-fission yields observed in adjacent-mass, asymmetric fission channels. Assuming that the ratio of complete to incomplete fusion-fission is the same as that observed for the evaporation residues (which may not be valid), then a total complete fusion-fission cross section of the order of 100 mb could be present.

In model calculations presented above the limitation on complete fusion originates from the inability of the largest partial waves to reach a critical distance of approach. Other possible limitations have been suggested. Fusion cross sections for the $^{28}Si + ^{28}Si$ and $^{16}O + ^{40}Ca$ systems have been calculated by Bonche, *et al.*[74] in the microscopic time-dependent Hartree-Fock (TDHF) approximation with a Skyrme interaction (Force I). This model reproduces the decreasing $^{16}O + ^{40}Ca$ cross sections above $E_{c.m.} = 100$ MeV reasonably well (see Fig. 3 of Ref. 74). The falloff corresponds to the occurrence of a low-l window which has yet to be verified experimentally. Moreover, the maximum angular momentum (60 units of $\hbar$) used in the fusion process is in disagreement with the recent fission-barrier calculations[68,75,76] which predicts a limit of approximately $43-48$ $\hbar$ for the ^{56}Ni compound nucleus. In the promptly emitted particles (PEP) and overlapping Fermi sphere models complete- and incomplete-fusion processes compete for the same partial waves.[47-50] If this is true then the cross sections predicted by angular-momentum limitation entrance-channel models discussed above overestimate the possible complete fusion cross section at higher bombarding energies.

VI. SUMMARY AND CONCLUSIONS

The reaction products resulting from central collisions in the $^{16}O + ^{40}Ca$ reaction at $E_{lab} = 13.4$ MeV/nucleon

have been studied to obtain information about fusion processes. Our time-of-flight measurements allowed extraction of the velocity distributions of the resolved evaporation-residue mass groups. The average linear-momentum transfer in the evaporation-residue Galilean-invariant velocity distributions was 88.6%, implying that only approximately 13.5 nucleons of the ^{16}O projectile are captured in the fusion process. The effects of anisotropic emission of evaporated light particles on the velocity distributions of the residues were examined in quantitative detail with evaporation codes. While anisotropic emission is predicted to have very little effect on the evaporation-residue velocity distributions observed at small laboratory angles (i.e.; $\theta_{\text{lab}} < 10°$), at larger angles the velocity centroids are shifted significantly to lower velocities. This must be taken into account when the velocity-deficit fraction is used to extract information about the linear-momentum transfer.

One of the motivations for the present study was to understand the large evaporation-residue cross sections that had been reported for this reaction at high bombarding energies. Guided by Monte Carlo simulations of the complete fusion, cross section limits for various processes were established. Of the 965±100 mb of cross section observed for reaction products with mass $32 \leq A \leq 52$, about 200 mb is identified with yields whose kinematics are inconsistent with evaporation residues (and indicative of binary processes; i.e., deep-inelastic scattering or fusion followed by fission), a lower limit of 230 mb is identified with incomplete-fusion processes, and an upper limit of about 528 mb is identified as consistent with evaporation residues from complete fusion. Based on model simulations of complete fusion-incomplete fusion sources, the upper limit for complete fusion is reduced to 475 mb.

The broad angular distributions associated with residue yields consistent with complete fusion are interpreted as evidence for the presence of heavy particle ($A > 4$) evaporation or very mass asymmetric fission with cross sections on the order of 100 mb. Measurements of reaction products in the mass range $20 \leq A \leq 28$ show that about 100 mb of cross section are consistent with a more symmetric fusion-fission process. The relative contributions of complete and incomplete fusion to these fission yields could not be established.

Comparisons of two- and multi-source model simulations for complete and incomplete fusion with the observed linear-momentum deficits, angular distributions, and mass distribution allowed constraints to be put on the character and relative magnitudes of the contributing incomplete fusion processes. Two-source model simulations showed that the angle dependence of the velocity-deficit fraction for any particular mass depends on the velocities, the relative strengths, and the emission anisotropies of the different contributing sources. The major features in the data can be reproduced in the framework of these calculations with the assumption of single- (two) nucleon and alpha-particle preequilibrium emission and a corresponding reduction in the complete-fusion cross section. Complete-fusion cross sections less than 475 mb and incomplete-fusion cross section greater than 300 mb are implied from the comparisons. The uncertainties in the predicted properties of the complete-fusion evaporation residues constitute the major obstacle for using the procedures outlined in this paper for a better estimate of the relative complete and incomplete yields. Comparisons with light-particle evaporation-residue coincidence results are needed to verify the model predictions.

The upper limit for the complete-fusion evaporation-residue cross section extracted in this study is consistent with the expectations based on recent fission-barrier calculations. Comparisons with results reported for the ^{32}S$+^{24}$Mg and ^{28}Si$+^{28}$Si reactions show that the evaporation-residue cross sections for the symmetric entrance-channel reactions are larger than expected. Further measurements are needed to determine whether the observed differences reflect an entrance-channel dependence of the fission barriers or the presence of incomplete-fusion processes whose contributions to the evaporation residue have been misidentified previously. These measurements are also necessary to address the interesting question of whether an entrance-channel dependence for incomplete-fusion processes exists. Additional measurements that would establish the fusion-fission cross section behavior as a function of bombarding energy for the ^{16}O$+^{40}$Ca reaction and for the symmetric entrance-channel reactions are needed for understanding the fission-barrier dependence and the limitations imposed on the complete-fusion process.

ACKNOWLEDGMENTS

---

[1]Y. Chan, C. Albiston, M. Bantel, A. Budzanowski, D. DiGregorio, R. G. Stokstad, S. Wald, S. Zhou, and Z. Zhou, in Proceedings of the Symposium on The Many Facets of Heavy-Ion Fusion Reactions, Argonne, 1985 [Argonne National Laboratory Report No. ANL-PHY-86-1, 1986].

[2]V. E. Viola, in Proceedings of the Symposium on The Many Facets of Heavy-Ion Fusion Reactions, Argonne, 1985 [Argonne National Laboratory Report No. ANL-PHY-86-1, 1986].

[3]J. Galin, in Proceedings of the Symposium on The Many

Facets of Heavy-Ion Fusion Reactions, Argonne, 1985 [Argonne National Laboratory Report No. ANL-PHY-86-1, 1986].

[4]R. Vandenbosch, in *Nuclear Science Research Conference Series*, Vol. 6 of *Nuclear Physics with Heavy Ions*, edited by P. Braun-Münzinger (Harwood Academic, 1984), p. 447.

[5]Ch. Gregoire and B. Tamain, Ann. Phys. (Paris) **11**, 323 (1986).

[6]D. G. Kovar, *Proceedings of the 5th Adriatic International Conference on Nuclear Physics, Croatia, 1984* edited by N. Cintro, W. Greiner and R. Caplar (World Scientific, Singapore, 1984), pp. 185–204.

[7]S. E. Vigdor, D. G. Kovar, P. Sperr, J. Mahoney, A. Menchaca-Rocha, C. Olmer, and M. S. Zisman, Phys. Rev. C **20**, 2147 (1979).

[8]G. Rosner, D. G. Kovar, P. Chowdhury, D. Henderson, H. Ikezoe, R. V. F. Janssens, W. Kühn, G. S. F. Stephans, B. Wilkins, F. Prosser, Jr., J. J. Kolata, and J. Hinnefeld, Bull Am. Phys. Soc. **28**, 670 (1983); Argonne National Laboratory, Physics Division Annual Report No. ANL-83-25, 1983.

[9]J. D. Hinnefeld, J. J. Kolata, D. J. Henderson, R. V. F. Janssens, D. G. Kovar, K. T. Lesko, G. Rosner, G. S. F. Stephans, A. M. van den Berg, B. D. Wilkins, F. W. Prosser, and S. V. Reinert, Phys. Rev. C **36**, 989 (1987).

[10]S. B. Kaufman, E. P. Steinberg, B. D. Wilkins, J. Unik, A. J. Gorski, and M. J. Fluss, Nucl. Instrum. Methods **115**, 47 (1974).

[11]J. B. Moulton, J. E. Stephenson, R. P. Schmitt, and G. J. Wozniak, Nucl. Instrum. Methods **157**, 325 (1978).

[12]M. Ogihara, Y. Nagashima, W. Galster, and T. Mikumo, Nucl. Instrum. Methods **251**, 313 (1986).

[13]W. Bohne, W. Galster, K. Grabisch, and H. Morgenstern, Nucl. Instrum. Methods A **240**, (1985).

[14]R. Butsch, J. Pochodzalla, and B. Heck, Nucl. Instrum. Methods **228**, 586 (1985).

[15]D. H. Gloeckner, M. H. Macfarlane, and S. C. Pieper, PTOLEMY, Argonne National Laboratory Report No. ANL/PHY-76-11, 1976.

[16]J. Gomez Del Campo, R. G. Stokstad, J. A. Biggerstaff, R. A. Dayras, A. H. Snell, and P. H. Stelson, Phys. Rev. C **19**, 2170 (1979).

[17]Y. Chan, M. Murphy, R. G. Stokstad, I. Tserruya, S. Wald, and A. Budzanowski, Phys. Rev. C **27**, 447 (1983).

[18]V. Viola Jr., B. B. Back, K. L. Wolf, T. C. Awes, C. K. Gelbke, and H. Breuer, Phys. Rev. C **26**, 178 (1982).

[19]H. Ikezoe, N. Shikazono, Y. Tomita, K. Ideno, Y. Sugiyama, and E. Takekoshi, Nucl. Phys. **A444**, 349 (1985).

[20]J. Gomez Del Campo and R. G. Stokstad, Oak Ridge National Laboratory Technical Report No. ORNL-TM-7295, 1981.

[21]G. Rosner, J. Pochodzalla, B. Heck, G. Hlawatsch, A. Miczaika, H. J. Rabe, R. Butsch, B. Kolb, and B. Sedelmeyer, Phys. Lett. **150B**, 87 (1985).

[22]S. J. Sanders, R. R. Betts, I. Ahmad, K. T. Lesko, S. Saini, B. D. Wilkins, F. Videbaek, and B. K. Dichter, Phys. Rev. C **34**, 1746 (1986).

[23]S. J. Sanders, B. B. Back, R. R. Betts, B. K. Dichter, S. Kaufman, D. G. Kovar, B. Wilkins, and F. Videbaek, in Proceedings of the Symposium on The Many Facets of Heavy-Ion Fusion Reactions, Argonne, 1985 [Argonne National Laboratory Report No. ANL-PHY-86-1, 1986].

[24]V. E. Viola, K. Kwiatkowski, and M. Walker, Phys. Rev. C **31**, 1550 (1985).

[25]J. Töke, R. Bock, G. X. Dai, A. Gobbi, S. Gralla, K. D. Hildenbrand, J. Kuzminski, W. F. J. Müller, A. Olmi, H. Stelzer, B. B. Back, and S. Bjørnholm, Nucl. Phys. **A440**, 327 (1985).

[26]S. M Lee, W. Yokota, and T. Matsuse, in Proceedings of the Symposium on The Many Facets of Heavy-Ion Fusion Reactions, Argonne, 1985 [Argonne National Laboratory Report No. ANL-PHY-86-1 1986].

[27]S. J. Sanders, D. G. Kovar, B. B. Back, C. Beck, B. K. Dichter, D. Henderson, R. V. F. Janssens, J. G. Keller, S. Kaufman, T.-F. Wang, B. Wilkins, and F. Videbaek, Phys. Rev. Lett. **59**, 2856 (1987).

[28]J. Brzychczyk, K. Grotowski, Z. Majka, S. Micek, R. Płaneta, D. Fabris, K. Hagel, J. B. Natowitz, G. Nebbia, P. Belery, P. Cohilis, Y. El Masri, and Ch. Gregoire, Phys. Lett. B **194**, 473 (1987).

[29]K. Grotowski, Z. Majka, R. Płaneta, M. Szczodrak, Y. Chan, G. Guarino, L. G. Moretto, D. J. Morrissey, L. G. Sobotka, R. G. Stokstad, I. Tserruya, S. Wald, and G. J. Wozniak, Phys. Rev. C **30**, 1214 (1984).

[30]R. Płaneta, P. Belery, J. Brzychzyk, P. Cohilis, Y. El Masri, Ch. Gregoire, K. Grotowski, Z. Majka, S. Micek, M. Szczodrak, A. Wieloch, and J. Albinski, Phys. Rev. C **34**, 512 (1986).

[31]J. Hinnefeld, J. J. Kolata, D. G. Kovar, C. Beck, M. F. Vineyard, D. Henderson, R. V. F. Janssens, K. T. Lesko, A. Menchaca-Rocha, F. W. Prosser, S. J. Sanders, G. S. F. Stephans, and B. D. Wilkins, Argonne National Laboratory Report No. ANL-87-13, 1987.

[32]PACE is the modification of the code JULIAN described by A. Gavron, Phys. Rev. C **21**, 230 (1980).

[33]H. Morgenstern, W. Bohne, K. Grabisch, H. Lehr, and W. Stoffler, Z. Phys. A **313**, 39 (1983).

[34]J. Pochodzalla, R. Butsch, B. Heck, and G. Rosner, Phys. Lett. B **181**, 33 (1986).

[35]L. G. Sobotka, M. L. Padgett, G. J. Wozniak, G. Guarino, A. J. Pacheco, L. G. Moretto, Y. Chan, R. G. Stokstad, I. Tserruya, and S. Wald, Phys. Rev. Lett. **51** 2187 (1983); L. G. Sobotka, M. A. McMahan, R. J. McDonald, C. Signarbieux, G. J. Wozniak, M. L. Padgett, J. H. Gu, Z. Q. Yao, and L. G. Moretto, Phys. Rev. Lett. **53**, 2004 (1984).

[36]W. Mittig, A. Cunsolo, A. Foti, J. P. Wieleczko, F. Auger, B. Berthier, J. M. Pascaud, J. Quebert, and E. Plagnol, Phys. Lett. **154B**, 259 (1985); F. Auger, B. Berthier, A. Cunsolo, A. Foti, W. Mittig, J. M. Pascaud, E. Plagnol, J. Quebert, and J. P. Wieleczko, Phys. Rev. C **35**, 190 (1987).

[37]T. Kozik, J. Buschmann, K. Grotowski, H. J. Gils, N. Heide, J. Kiener, H. Klewe-Nebenius, H. Rebel, S. Zagromski, A. J. Cole, and S. Micek, Z. Phys. A **326**, 421 (1987).

[38]L. G. Moretto, in Proceedings of the Symposium on The Many Facets of Heavy-Ion Fusion Reactions, Argonne, 1985 [Argonne National Laboratory Report No. ANL-PHY-86-1, 1986].

[39]U. L. Businaro and S. Gallone, Nuevo Cimento 1, 629 (1955); 1, 1277 (1955).

[40]M. Blann, Phys. Lett. **88B**, 5 (1979).

[41]M. Blann, Phys. Rev. C **21**, 1770 (1980).

[42]B. K. Dichter, P. D. Parker, S. J. Sanders R. R. Betts, and S. Saini, Phys. Rev. C **35**, 1304 (1987).

[43]H. Morgenstern, W. Bohne, W. Galster, and K. Grabisch, Phys. Rev. Lett. **52**, 1104 (1984).

[44]G. S. F. Stephans, D. G. Kovar, R. V. F. Janssens, G. Rosner, H. Ikezoe, B. Wilkins, D. Henderson, K. T. Lesko, J. J. Kolata, A. Szanto De Toledo, E. M. Szanto, and P. L. Gonthier, Phys. Lett. **161**, 60 (1985).

[45]A. Budzanowski, H. Dabrowski, Y. Chan, R. G. Stokstad, I. Tserruya, and S. Wald, Phys. Rev. C **32**, 1534 (1985).

[46]H. Morgenstern, W. Bohne, K. Grabisch, D. G. Kovar, and

H. Lehr, Phys. Lett. **113B**, 463 (1982).

[47]J. P. Bondorf, J. N. De, A. O. T. Karvinen, G. Fai, B. Jakobsson, Phys. Lett. **84B**, 162 (1979).

[48]K. Möhring, W. J. Swiatecki, and M. Zielinska-Pfabe, Nucl. Phys. **A440**, 89 (1985).

[49]M. Blann, Phys. Rev. C **31**, 295 (1985).

[50]M. Blann, Phys. Rev. C **31**, 1245 (1985).

[51]H. Tricoire, Z. Phys. A **312**, 221 (1983); **317**, 347 (1984).

[52]Ch. Gregoire, and F. Scheuter, Phys. Lett. **146B**, 21 (1984).

[53]S. Leray, O. Granier, C. Ngo, E. Tomasi, C. Cerruti, P. L'Henoret, R. Lucas, C. Mazur, M. Ribrag, J. L. Charvet, C. Humeau, J. P. Lochard, M. Morjean, Y. Patin, L. Sinopoli, J. Uzureau, D. Guinet, L. Vagneron, and A. Peghaire, Z. Phys. A **320**, 533 (1985).

[54]C. Cerruti, D. Guinet, and A. Demeyer, Z. Phys. A **321**, 633 (1985).

[55]C. Ngo and S. Leray, Z. Phys. A **322**, 419 (1985).

[56]J. B. Natowitz, S. Leray, R. Lucas, C. Ngo, E. Tomasi, and C. Volant, Z. Phys. A **325**, 467 (1986).

[57]J. Randrup and R. Vandenbosch, Nucl. Phys. **A474**, 219 (1987).

[58]J. Wilczynski, K. Siwek-Wilczynska, J. Van Driel, S. Gonggrijp, D. C. J. M. Hageman, R. V. F. Janssens, J. Lukasiak, R. H. Siemssen, and S. Y. Van Der Werf, Nucl. Phys. **A373**, 109 (1982).

[59]C. Gershel, Nucl. Phys. **A387C**, 297 (1982).

[60]H. Morgenstern, W. Bohne, W. Galster, and K. Grabisch, Z. Phys. A **324**, 443 (1986).

[61]I. Tserruya, V. Steiner, Z. Fraenkel, P. Jacobs, D. G. Kovar, W. Henning, M. F. Vineyard, and B. G. Glagola, Phys. Rev. Lett. **60**, 14 (1988).

[62]See Proceedings of the International Conference on Heavy Ion Nuclear Collisions in the Fermi Energy Domain, Caen, 1986 [J. Phys. C **4**, (1986)].

[63]Y. Nagashima, J. Schimizu, T. Nakagwa, Y. Fukichi, W. Yokota, K. Furono, M. Yamanouchi, S. M. Lee, N. X. Dai, T. Mikumo, and Y. Motobayashi, Phys. Rev. C **33**, 176 (1986).

[64]S. B. DiCenzo, J. F. Peterson, and R. R. Betts, Phys. Rev. C **23**, 2561 (1981).

[65]H. H. Gutbrod, W. G. Winn, and M. Blann, Nucl. Phys. **A213**, 267 (1973).

[66]D. G. Kovar, P. D. Bond, C. Flaum, M. J. Levine, and C. E. Thorn, Bull. Am. Phys. Soc. **22**, 66 (1977); D. G. Kovar, in Proceedings of the IPCR Symposium on Macroscopic Features of Heavy Ion Collisions and Preequilibrium Processes, Hakone, 1977 [IPCR Cyclotron Prog. Rep. Suppl. **6**, 18 (1977)].

[67]A. J. Sierk, Phys. Rev. Lett. **55**, 582 (1985).

[68]A. J. Sierk, Phys. Rev. C **33**, 2039 (1986).

[69]J. R. Birkelund, L. E. Tubbs, J. R. Huizenga, J. N. De, and D. Sperber, Phys. Rep. **56**, 107 (1979); J. R. Birkelund and J. R. Huizenga, Ann. Rev. Nucl. Part. Sci. **33**, 265 (1983).

[70]P. Fröbrich, Phys. Rep. **116**, 337 (1984).

[71]T. Matsuse, A. Arima, and S. M. Lee, Phys. Rev. C **26**, 2338 (1982).

[72]S. M. Lee, and T. Matsuse, J. Phys. Soc. Jpn. **54**, 272 (1985); T. Matsuse and S. M. Lee, Proceedings of Tsukuba International Symposium on Heavy Ion Fusion Reaction, Tsukuba, 1984 (unpublished).

[73]L. G. Moretto, Nucl. Phys. **A247**, 211 (1975).

[74]P. Bonche, K. T. R. Davies, B. Flanders, H. Flocard, B. Grammaticos, S. E. Koonin, S. J. Kriger, and M. S. Weiss, Phys. Rev. C **20**, 641 (1979).

[75]M. G. Mustafa, P. A. Baisden, and H. Chandra, Phys. Rev. C **25**, 2524 (1982).

[76]M. Blann, Phys. Rev. C **34**, 2215 (1986).